POLITECNICO DI MILANO

Facolta di Ingegneria Dei processi Industriali

Dipartimento di Chimica, Materiali e Ingegneria Chimica “Giulio Natta”

HYDROGEN DIFFUSION IN PIPELINE STEELS

Relatore: Prof. Fabio Maria Bolzoni.

Correlatore: Ing. Ehsan Fallahmohammadi

Student:

Ejim Francis Okwudiri.

Mat n. **753154**

A.A. 2010/2011

ACKNOWLEDGEMENTS

First I would like to thank my major advisor, a PHD student on same research, Engr. Ehsan Fallahmohammadi, who guided me through the learning process of conducting a well planned and executed research work.

My special thanks go to G. Fumagalli and G. Re, my co-advisors, for their invaluable comments and encouragements throughout the research.

The guidance and challenge from my relatore Prof. Fabio Maria Bolzoni cannot be over emphasized. He shaped me into a better researcher, which will benefit me throughout my life.

Finally, and most importantly, I would like to thank my parents and my brothers for their prayers.

There are no appropriate words that can express my gratitude to them for their sacrifice, love and support.

Thank you all.

Table of contents

Chapter 1: Introduction

In the presence of hydrogen sulphide (H_2S), metallic materials, such as carbon and low alloy steels, may suffer hydrogen damage and hydrogen embrittlement. Moreover, reduction of toughness and ductility due to hydrogen adsorption may occur.

In a previous phase of this research, an electrochemical method to charge large specimens with hydrogen has been set up; diffusible hydrogen content was measured in the range 0.6 to 2 ppm. The specimens charged with hydrogen were submitted to mechanical testing: hydrogen significantly affected the fracture toughness of the tested steels; these findings were confirmed by the fracture surface examination after mechanical testing.

The evaluation of the kinetics of hydrogen adsorption, entry and transport process in steel, under the given set of conditions, is required to increase knowledge of the mechanisms and factors controlling hydrogen embrittlement phenomena. Once it has entered the metal, hydrogen can induce embrittlement and finally cause the failure of the material.

In general, one may distinguish the following processes in a metal-hydrogen system:

(i) the entry of hydrogen from the surrounding environment into the metal,

(ii) the transport (diffusion) of hydrogen inside the metal and

(iii) the trapping of hydrogen at structural defects and/or formation of hydrides phases.

Many studies have been reported in literature on hydrogen permeation of steel membranes, including the analysis of hydrogen trapping defects. In most cases the electrochemical method of Devanathan has been employed largely because of its high sensitivity and versatility at room temperature and because it requires simple electrochemical equipment.

The technique involves locating the metal specimen between the charging and oxidation cell. Hydrogen atoms are generated in the charging cell through corrosion or cathodic protection. Diffuse through the metal and are oxidized electrochemically on exiting the other side of the specimen. The time variation of this hydrogen oxidation current is referred to as the permeation transient.

The scope of the work carried out in this thesis is to study in detail the hydrogen permeation processes in the pipeline materials, in order to present a practical approach for the effective use of the established technique in estimating the permeation parameters through a carbon and a low alloy steels for pipeline (API 5L X65 and ASTM A182 F22). In this work, test have been carried out at a temperature 40°C. The results of this thesis have been compared with those obtained in a previous work carried out at 20°C.

Chapter 2: Hydrogen Embrittlement and Cracking

2.1 Introduction

There are several ways in which hydrogen can be absorbed by metal from aqueous environments, such as electroplating, acid pickling, cathodic protection, etc.

When atomic hydrogen diffused into a metal and remains in solid solution within the lattice of the metal, it reduces the ductility and formability of the metal. This is known as hydrogen embrittlement. Hydrogen ion reduction reaction is written as follows:

$2H^+ + 2e^- \leftrightarrow H_2$ (takes place in acid environments)

$H^+ + e^- \leftrightarrow H_{ads}$ (atomic hydrogen H_{ads} adsorbed onto the metallic surface)

This atomic hydrogen (H_{ads}) may penetrate into the metal's crystal lattice or form hydrogen molecule H_2 by the recombination ($H_{ads} + H_{ads} \leftrightarrow H_2$). The direction of reaction depends on the availability of specific poison on the surface of the metal to inhibit the later. The presence of H_2S give rise to poisoning as described in section 3.2.1, leading to accumulation of hydrogen atom in the metal establishing some forms of cracking namely, stress corrosion cracking (SCC) due to hydrogen embrittlement, sulphide stress cracking (SSC) and another group of cracking that does not necessarily occur in the presence of externally applied or residual stresses e.g. hydrogen induced cracking (HIC) (blistering), stepwise cracking (SWC).

Stress corrosion cracking (SCC) is a phenomenon illustrating the formation and propagation of cracks in metals subjected to a combined action of tensile mechanical stresses and a corrosive environment. Tensile stresses may result from external applied force on the metal, but also could be from internal stresses, such as residual stresses during mechanical workings, welding or / and heat treatment operations [15].

Sulphide Stress Cracking (SSC): In the presence of stress, the embrittled metal readily cracks, depending on a lot of factors including composition of the steel, heat treatment, microstructure, mechanical resistance, temperature, time, pH, the applied load, partial pressure of H_2S, etc. The cracking process can be very rapid, and can cause catastrophic failure [14]. High yield microstructure increases the tendencies of SSC, so it is a kind of limiting factor to the strength which the steel can posses, according to ISO 15156 [15].

Stepwise cracking (SWC): Are small blisters connected by ductile tearing (step). As the name implies, the cracks and surface blisters have a characteristic stepped appearance. These cracks can occur in the absence of external applied or residual stress and appear parallel to the rolling plane of the steel plate. Such cracks occur when atomic hydrogen diffuses into the metal and recombines to form hydrogen molecules, which due to it large size cannot diffuse through the metal lattice, thereby creating a pressure at the trap sites of the steel matrix. As more hydrogen

atoms enter the steel, the pressure rises, deforming the surrounding steel so that the blisters become visible. At first the cracks are initiated and then propagate along the metallurgical structures sensitive to hydrogen embrittlement. These cracks are known as HIC, internal cracking, blistering etc. These cracking will continue to develop till failure of the steel structure, which can arise within months, if the corrosion is not stopped [14].

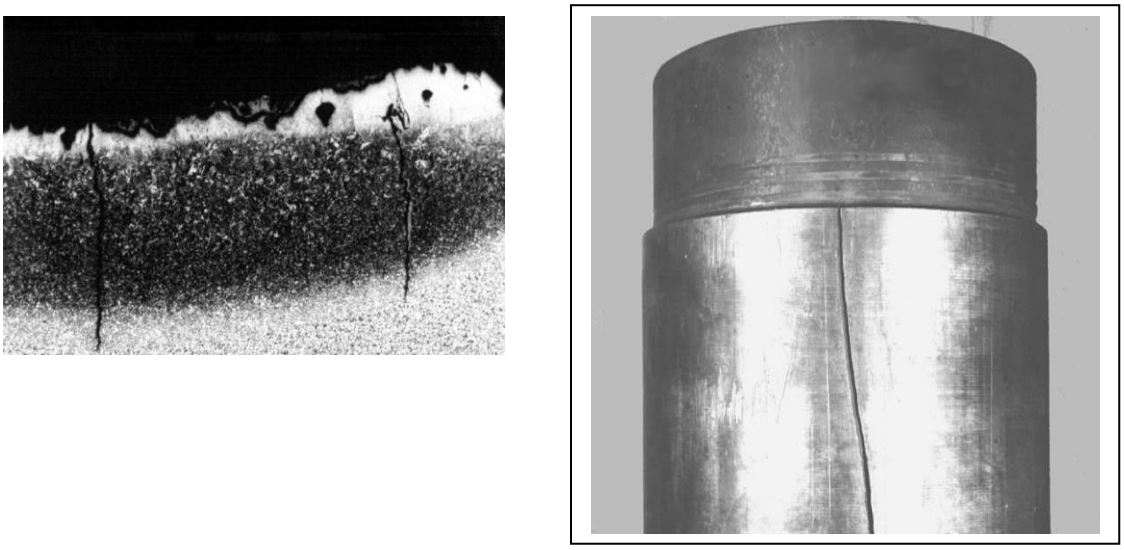

Figure 1: Two images of sulphide stress cracking [41]

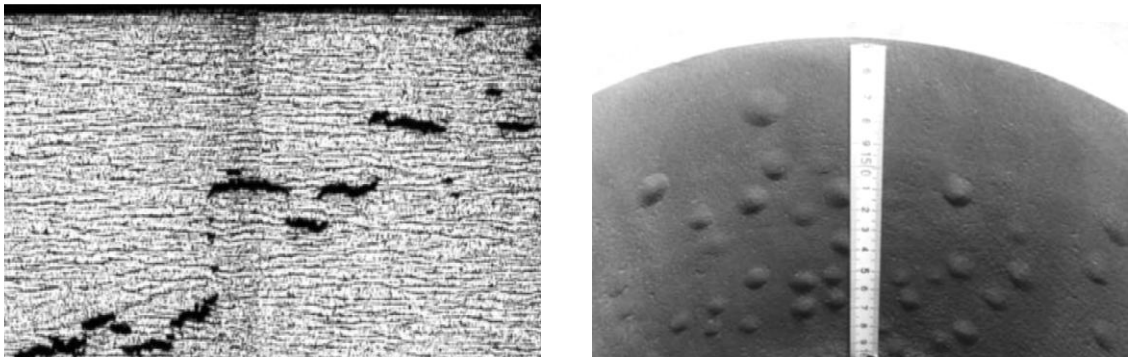

Figure 2: Two images of hydrogen induced cracking and blistering [41]

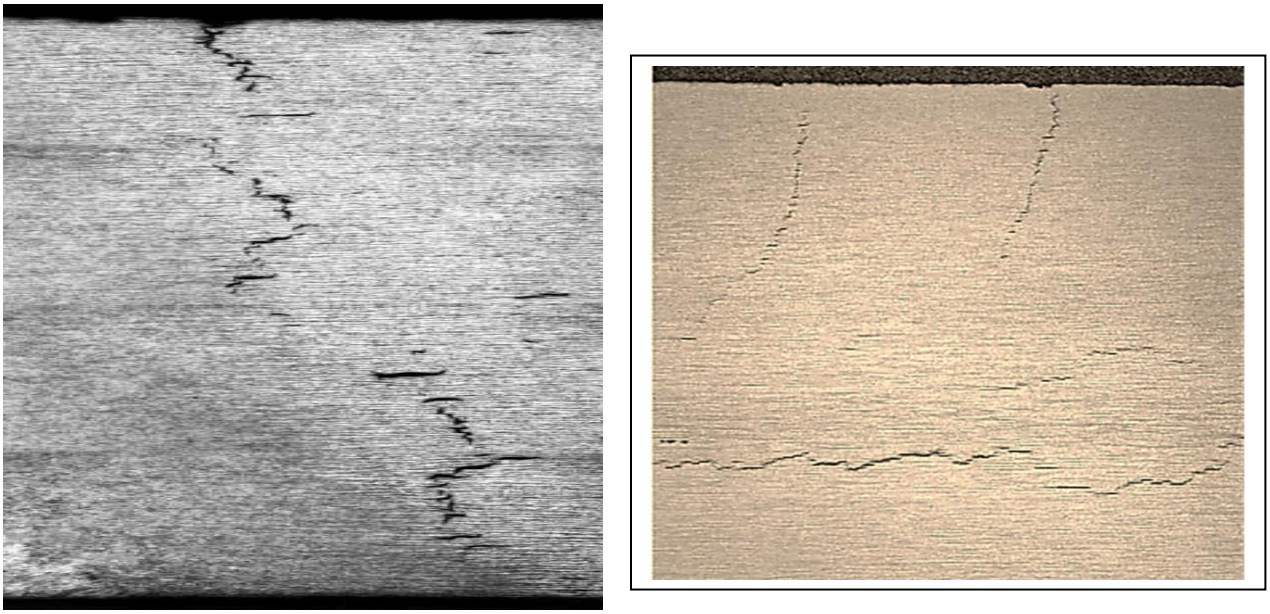

Figure 3: Two images of SOHIC [41]

Stress oriented hydrogen induced cracking (SOHIC) and soft zone cracking (SZC) are another group of cracking that lie in-between SSC and SWC. SOHIC is characterized by staggered small cracks formed approximately perpendicular to the principal, applied or residual stress, resulting in a ladder-like crack array.

SOHIC is caused by the combination of external stresses and the local straining around hydrogen induced crack; this has been observed in parent materials of longitudinally welded pipe. When these same characteristics are observed around the softened heat affected zone of a weld in rolled plate steel, it is called SZC [14].

2.2 Oil and Gas: Sour Environments

The simplest definition of sour environment is the one according to NACE standard (2003), which states that a sour environment is one in which the partial pressure of H_2S and the concentration of H_2S exceeds a given threshold, as a function of the type of fluid and the operating conditions [15]. Hydrogen up-take is dependent upon several parameters, but to mention the most important ones are hydrogen sulphide concentration, the operating pH and temperature. A general guideline for the occurrence of SSC in terms of pH and H_2S partial pressure, for oil country tubular goods (OCTG) materials up to grade P110 and the gas wells are given in figure 4 and 5.

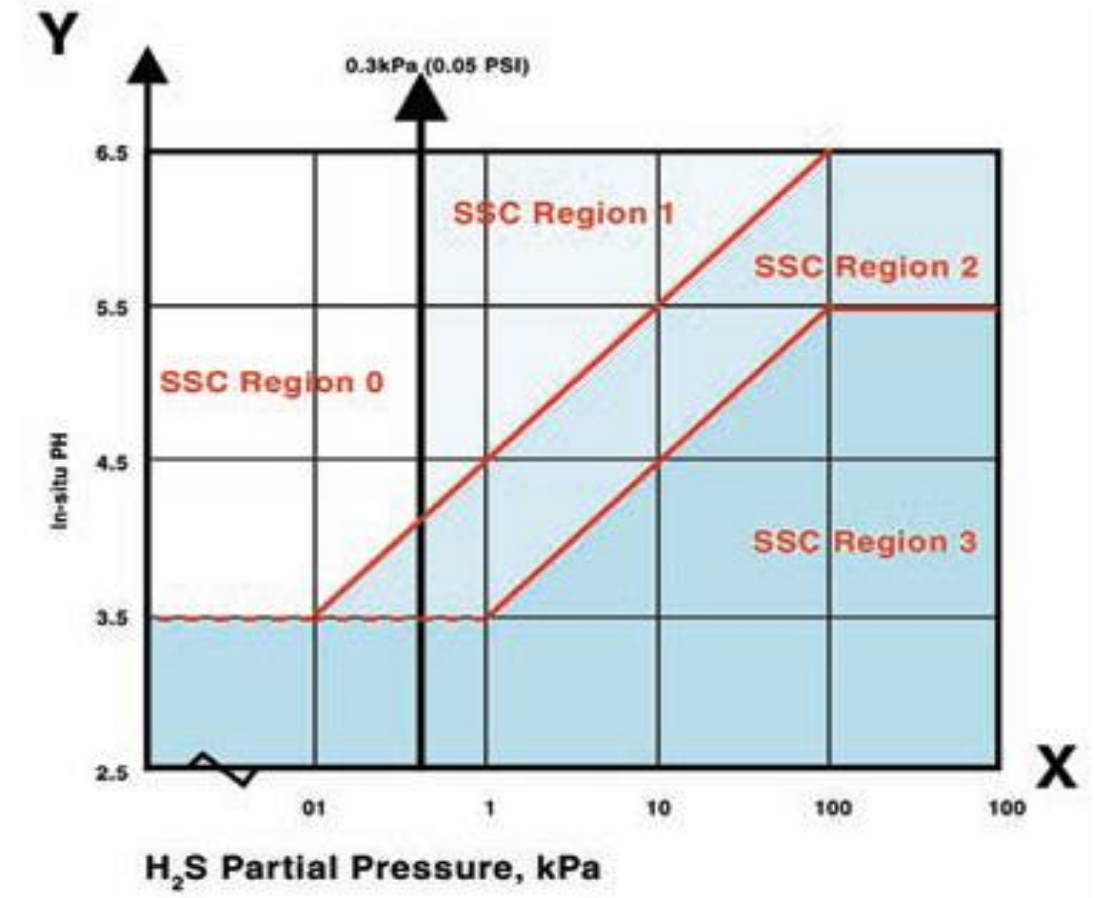

Figure 4 : Sulphide stress corrosion cracking domains as a function of pH and hydrogen sulphide partial pressure [14]

Four different regions are given in Fig. 4.

Region 0: Above the thresh hold pH (3.5) no forms of SSC is noticed.

Region 1: No form of SSC was observed for materials up to strength P110, at low H_2S partial pressure and high pH.

Region 2: This region is called the transition zone. In this region some judgments are required regarding the critical metallurgical requirements. Depending on the circumstance, the controlling factor in this region is whether the material is fit for the purpose or not.

Region 3: This is the domain of SSC. The steel materials selected for use in this region should be resistant to SSC.

The region below pH 3.5, which serves as the threshold level, practically is a region where the threshold value of pH_2S is low, so it is not considered.

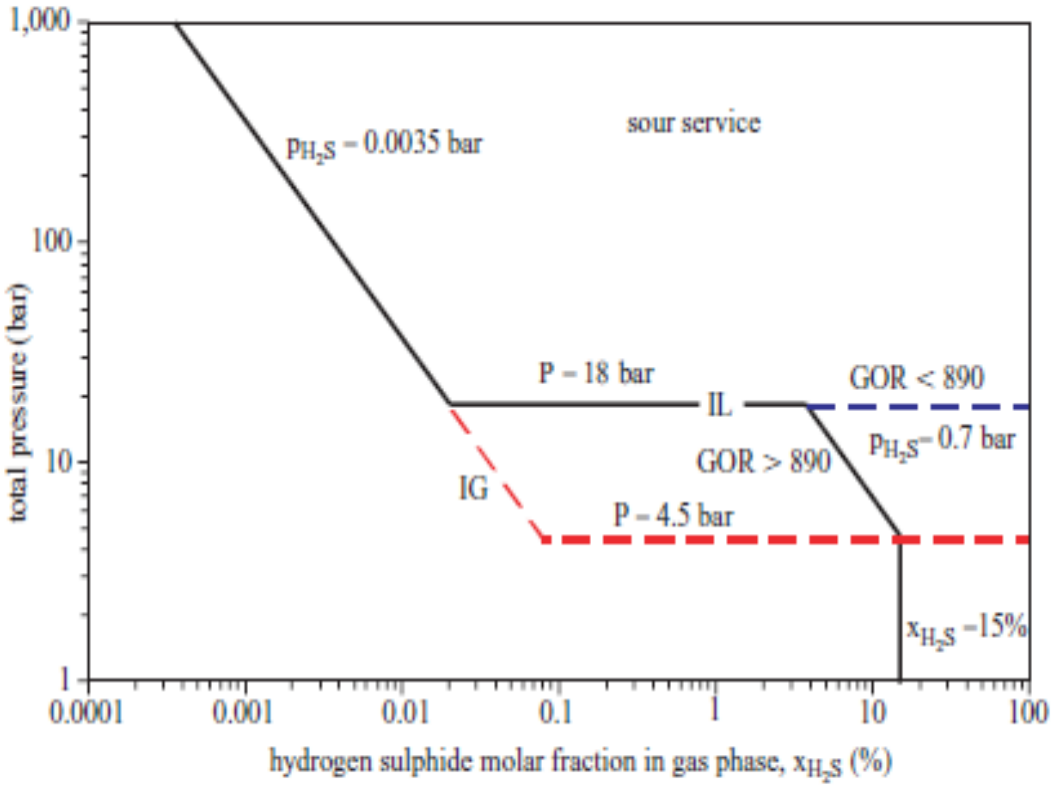

Figure 5: Identification of conditions for the onset of sulphide stress cracking (according to NACE, 2003) [15]

Figure 5 identify the region in which vulnerable steels and alloys are susceptible to SSC phenomenon in gas wells. The region above the partial pressure of 4.5 bar and the hydrogen sulphide molar fraction of 0.0035 bar is susceptible to SSC in gas wells [15].

2.3 Effect of hydrogen on mechanical properties of iron and steel

The destructive effects of hydrogen on the mechanical properties of iron and steels were first reported by W.H. Johnson in 1875 as the cause of reduction in ductility and fracture stress. This deterioration is known as hydrogen embrittlement. To a large extent it is believed that the physical and mechanical properties of metals, such as electrical resistance and ductility, are influenced by the extent of the irreversible changes in structure (blisters and cracks) brought about by the effect of hydrogen activities in the metal [19]. Other metals and alloys also undergo hydrogen embrittlement e.g. austenitic, martensitic and ferritic steels, nickel, titanium and aluminum alloys, but out of all these, the metal which is more severely affected is steel, especially steels with high strength because of their wide use in construction and apparatus exposed to the various aggressive environment.

Measurements of variations in the mechanical properties of a metal as induced by hydrogen (tensile and bending tests) are commonly used for the quantitative estimation of hydrogen embrittlement.

Some of the many proposed mechanisms to explain the observed effects of hydrogen on deformation and fracture include the internal pressure mechanism, in which the pressure of hydrogen in voids generates sufficient stress leading to nucleation and propagation of crack. Hydrogen adsorption at crack tips and on surface imperfections, which is the cause of reduction in surface energy. Hydrogen reduction of the cohesive strength of the lattice, which leads to de-cohesion, hydrogen accumulations at precipitates and second phase, which results in dislocation generation or crack nucleation and propagation. Reduction in the stacking fault energy by hydrogen, which increases the slip planarity, increase in density of strain induced vacancies by hydrogen stabilization, leading to the formation of micro cracks or voids. Hydrogen adsorption, which induces dislocation injection from surface and hydrogen, enhanced localized plasticity-the larger the initial strength of steel, the greater is the reduced plasticity [17].

In iron of different purity, hydrogen ingress could also cause the formation of brittle cracks. This is mainly because of hydrogen interaction with dislocations. In a research by H. Kimura, he reported that high pure iron softens with hydrogen charging, while less pure iron hardens instead, during hydrogen charging at room temperature. This is the result of hydrogen dislocation interaction; in that the hydrogen atoms trapped at the core of a screw dislocation increases its mobility and hinders the motion of the edge dislocations [18].

2.3.1 Critical Concentration of Hydrogen

Hydrogen atoms present in the iron in the form of dissolved hydrogen is responsible for the dilation of the metal lattice. As the concentration increases, the interaction with dislocations increases bringing about a peak in the internal friction, at critical hydrogen concentration, c_c. This is responsible for both physical effect like, the raising of the residual electrical resistivity, and mechanical-metallurgical effects like, reversible hydrogen embrittlement of polycrystalline iron, plastic deformation, decreased density, etc. c_c is the concentration at which micro-cracks and voids filled with molecular hydrogen develops in the metal [19].

In a recent study on annealed and cold worked up to 75% ZR membrane, the concentration of diffusible hydrogen is a linear function of the square root of the current density and until concentration range of up to 2.5 cm^3 H_2/100 g Fe, no blistering was observed in any of the methods used. For up to 89% cold worked iron, the critical concentration of hydrogen falls at 1.5 cm^3 H_2/100 g Fe, at an equilibrium pressure of molecular hydrogen pH_2=1.1 X 10^3 MPa. As the blisters are forming and developing the critical concentration of hydrogen decreases with increase in current density and the total concentration of hydrogen associated with the dislocations was found to be 3 cm^3 H_2/ 100 g Fe. While for Armco iron, the critical concentration

of diffusible hydrogen is found to be 0.03–0.04 cm^3 H_2/ 100 g Fe, at an equilibrium pressure of gaseous hydrogen range of 120 to 160 MPa.

2.3.2 Material Selection

In oil and gas environment often associated with hydrocarbons, the poison is the presence of H_2S, which is associated to SSC. In order to get the best materials that will not be susceptible to SSC, the following guidelines need to be followed.

SSC can be prevented by limiting the strength of the steel, in that way eliminating deleterious crack-sensitive microstructures. Measuring the bulk hardness is a convenient method to check the strength of OCTG and other non-welded components, having homogenous microstructures. Among the best bulk hardness test are Vickers HV30, Brinell and Rockwell. Whereas sites of microstructure in-homogeneities, as in weld zones with resulting tensile residual stresses, peak hardness and local hard zones are more important. Hence Vickers HV5 and HV10 or Rockwell 15N is the preferred methods for hardness testing across the welds [14].

The hardness at which steel is resistant to SSC depends on the severity of the environment. To this effect the guidelines for allowable hardness in mildly sour environment can be relaxed provided that appropriate tests show that the material will resist SSC. Note that materials which do not meet these requirements may still have good resistance to SSC but needs to be proven with appropriate tests.

Table 1: Acceptable Vickers hardness limits for welds [14].

Hardness Location	**Region 3** Sour service domain	**Region 2** Transition domain	**Region 1** $pH_2S > 0.0034$ bar $pH < 6.5$
Weld Metal and Heat Affected Zone:	-	-	-
Root and fill	250	280	300
Cap (wall ‹ 9.5 mm thick)	275	300	325
Cap (wall ≥ 9.5 mm thick)	300	325	350

In piping, pressure vessels and other welded components, the hardness should not exceed 250 HV30. Distinction should be made, depending on the direction of flow of hydrogen, between the values of hardness of the inner and outer surface (wall). Since the hydrogen concentration is less severe at the outer side, higher hardness in the final cap pass of the weld and heat affected zone (HAZ) are allowed [14].

Cold rolled forging or working during fabrication may lead to SSC susceptibility of carbon or low alloy steel at hardness below 250 HV [14].

SWC susceptibility can be controlled through the material properties of the steel. The use of coatings, cladding and inhibitors may in some operational circumstances be adequate solutions. During production, the steels within this group can be made with adequate SWC resistance by limiting sulphur content, shape controlling of inclusions, minimizing segregation, minimizing carbon, manganese and phosphorus as far as consistence with mechanical properties required [14].

Chapter 3: Hydrogen Transport in Metals

3.1 Introduction

In this chapter, we will discuss in addition to the electrochemical evolution of hydrogen, the solubility of hydrogen in iron, and hydrogen diffusion in metal without and with traps, reiterating points from literature on its mathematical modeling.

Hydrogen entry into iron and steel depends on a lot of environmental factors, like the potential of the electrolytes-metal interface, the current density of hydrogen evolution, the electrolyte composition and the pH of the surrounding electrolyte. Some substance acts as accelerators of this process, these substances are called promoters, while some others prevent this process and they are called inhibitors. The mechanisms of hydrogen entry into steel and the effect of promoters and inhibitors are still not very clear. This is undoubtedly due to the complexity of the metal-aqueous electrolyte boundary. Generally, the entry of hydrogen into steel, constitute one stage of a complex process which involves the conversion of the hydrogen, in the form of hydrated proton or of a water molecules in electrolyte, into dissolved hydrogen in metal. We will discuss about the rest of the stages as we progress.

The concentration of hydrogen just beneath the surface of the metal, which is in contact with the electrolyte, could be referred to as rate of hydrogen entry into the metal. The value of this concentration, since it cannot be measured directly, is obtained by measuring other quantities, namely:

a) The quantity of hydrogen adsorbed by the specimen over a certain period

b) The extent of physical and mechanical properties distortion by hydrogen

c) The permeation rate of hydrogen through the membrane.

The results obtained from these measurements are not always equal and usually do not represent the quantitative characteristics of hydrogen entry itself because hydrogen entry also equally depends on the shape of the specimen and the time of hydrogen charging. In addition to the problems in determining the concentration of hydrogen just beneath the surface of the metal, is also the fact that the hydrogen absorbed by iron and steel may occur at least in three different forms, namely:

I. Hydrogen in the interstitial solid solution

II. Hydrogen connected with structural defects, e.g. in dislocations

III. Molecular hydrogen accumulated in the crevices and blisters

3.2 Electrochemical Evolution of hydrogen

In order to determine the mechanism of hydrogen evolution reaction in an electrochemical desorption, it is first necessary to know whether the discharge reaction is hydrogen ions or water molecules.

Hydrogen evolution occurs in two stages; first stage, hydrogen adsorption; consist of the discharge of hydronium ions or water (D).

In acid solution $H_3O^+ + M + e \rightarrow MH_{ads} + H_2O$

In alkaline solution $H_2O + M + e \rightarrow MH_{ads} + OH^-$

Second stage, electrochemical desorption (ED); consist of the formation of adsorbed hydrogen atoms MH_{ads},

In acid solution $MH_{ads} + H_3O^+ + e \rightarrow H_2 + H_2O + M$

In alkaline solution $MH_{ads} + H_2O + e \rightarrow H_2 + OH^- + M$

Each of the stages in electrochemical desorption may have different rates, here it is assumed that the fast stage is at equilibrium, meaning that the rate of forward reaction is equal to the reversed one, the slowest stage controls the overall reaction and determines the overpotential.

Slow discharge, fast electrochemical desorption $H_3O^+ \xrightarrow{D} MH_{ads} \underset{}{\overset{ED}{\rightleftharpoons}} H_2$

Fast discharge, slow electrochemical desorption $H_3O^+ \overset{D}{\rightleftharpoons} MH_{ads} \xrightarrow{ED} H_2$

On the basis of electrochemical parameters such as the Tafel slope, the coverage of the electrode surface by hydrogen atoms, the exchange current density, the transfer coefficient or the stoichiometric number, it can be established which of the above mechanisms is probable. The results of electrochemical measurement, however, are affected by an additional factor (current density, electrolyte composition) and often are inconsistent. Due to these effects and including the fact that in iron and its alloys, evolution and absorption occurs simultaneously, has lead to a lot of discrepancies in electrochemical results available in literature [19]. Therefore, it is not surprising the discrepancies recorded in literature.

3.2.1 Promoters of Hydrogen Absorption

Certain substances referred to as promoters of hydrogen entry, when present in the electrolyte even in small quantities, may significantly accelerate the process of the cathodic hydrogen entry into the metal. The most effective promoters are compounds of certain elements of group V (P, As, Sb, Bi) and group VI (S, Se, Te) of the periodic table. In oil and gas environment S is present

in the form of H_2S. Hydrogen absorption is enhanced in environment containing $H_2S/HS^-/S^{2-}$, but reduces at a higher pH above pH 7. Angerstain-Kozlowska [19] reported that the addition of As_2O_3 to 0.2 M H_2SO_4 accelerates hydrogen entry only at potentials that are more negative than the potential at which arsenic begins to reduce to arsine. The surface of the iron cathode is covered by a film of arsenic deposition at a more positive potential, this film protects the metal against corrosion but also reduces the entry of hydrogen into the metal. Also sodium sulphide hydrolyzes with evolution of hydrogen sulphide, thereby increasing permeation at potentials as low as corrosion potential [19]. A recent research by Enkela Nocka [19], on hydrogen permeation in carbon steel, inhibitors and promoters impact, while employing the Devanathan electrochemical technique, investigated the effects of five different promoters, namely Aniline, Formaldehyde, Benzonitril, Urotropine and p-Toluidine, on 12% HCl and HCl + Na_2S electrolyte-carbon steel interface. He reported that the result clearly shows that Na_2S promotes hydrogen permeation strongly, while Urotropine among the organic compounds shows the most inhibitive effects on the Na_2S activities [22].

Ramunni [19] reported from literature some concepts related to the mechanism of promoters activities. The first concept attributed the accelerating effect of promoters to poisoning of the recombination reaction of the adsorbed hydrogen atoms into molecules, thereby leading to increase concentration of atomic hydrogen on the cathodic surface. A second concept is based on the promoters' ability to lower the M-H_{ads} bond energy, resulting in the decrease of activation energy for the process of passage of hydrogen atoms from surface into the metal phase. Other hydrogen absorption promoters includes, thiosulphate ($S_2O_3^{2-}$) and in acid solution, sulphite (SO_3^{2-})

3.3 Solubility of hydrogen in iron

Dissolution and occlusion of hydrogen by iron in its simplest term is the power of iron and steel to dissolve and shut up hydrogen. It is evident that the solution of hydrogen atom in the metal lattice is not by substitution. Several authors has demonstrated by neutron diffraction that hydrogen occupies interstitial positions in metal lattices e.g. the face centered cubic (FCC) lattice has one octahedral interstitial site per metal atom (at ½, 0, 0 and equivalent positions), and two tetrahedral interstitial sites per metal atom (at ¼, ¼, ¼ and equivalent positions). The body centered cubic (BCC) lattice has three octahedral interstitial sites per metal atom (at the centers of the cube faces and on the cube edges) and six tetrahedral interstitial sites per metal atom (at ½, ¼, 0 and equivalent positions). In the F.C.C lattice the octahedral positions has the largest free volume, whereas in the B.C.C lattice the tetrahedral sites are the largest [3]. Alpha (α) iron of body centered cubic (BCC) lattice, having octahedral and tetrahedral interstitials within the crystal lattice with a space filling of 68%. In gaseous phase, the overall reaction of dissolution in iron is endothermic and the heat of dissolution Q value, at temperatures from 573 to 1173 °K are obtained in the range 22.0 to 30.8 KJ mol^{-1} [19]. At a constant pressure of gaseous hydrogen

(pH_2) and various temperatures, the solubility, S found can be used to calculate the heat (enthalpy) of dissolution of hydrogen according to this relation:

$$S = S_0 \exp(^{-Q}/_{RT}) \quad (1)$$

Where S_0 is an approximately constant quantity, R is the gas constant and T is the temperature of the system. Sieverts law gives the relation of the pressure of molecular hydrogen on the solubility of this gas in the metal. This is expressed as the square-root formula;

$$S = S_1\sqrt{pH_2} \quad (2)$$

A studies on the dissolution of hydrogen in mono- and polycrystalline zone-refine (ZR) iron of variable purity have shown that the solubility S of hydrogen in this iron is partially dependent on the chemical composition of the metal at temperatures above 573 °K, but at temperatures above 673 °K, the effects of grain boundaries is not felt. Oriani explained the deviation of equation 1 in terms of

$$\log S = f(^1/_T), \quad (3)$$

stating that there is a temperature dependent degree of occupation of tetrahedral and octahedral interstitials in metal by hydrogen. At elevated temperature between 273 and 333 °K and pressure range of 3×10^{-3} to 50 MPa, following the study of hydrogen permeation rate through ZR iron membrane coated with a thin palladium layer, it was confirmed that the solubility of hydrogen in metal is proportional to the square root of the pressure of the gas. Still according to Oriani, the effect of temperature and fugacity on the solubility is given by this equation:

$$S = 47f^{0.5} \exp\left(-\frac{27200}{RT}\right) \quad (4)$$

Where f is the fugacity and S, the solubility is given in cm^3H_2/100 g Fe. Such that, when calculations of solubility of hydrogen are needed at high pressure and room temperature, the fugacity of the gas is used [19].

The principle behind the measurement of hydrogen solubility S in a metal consist of quantifying the amount of absorbed hydrogen gas in a specimen of known weight, at a constant, partial pressure of the gaseous hydrogen pH_2 and temperature, after attaining equilibrium position in the system [19]. As stated above, solubility studies of hydrogen are much more accurate, when carried out at elevated temperature. At temperatures below 573 °K, studies have shown that the results are unreliable. This is due to the low solubility of hydrogen in iron, the difficulties of eliminating the effect of surface processes and the possible interaction of hydrogen with defects of the host lattice of the metal.

To this effect the temperature dependence of solubility in iron is shown in figure 6 with respect to α, δ (BCC) iron, γ (FCC) iron and liquid iron (l) at pH_2 = 1 atm.

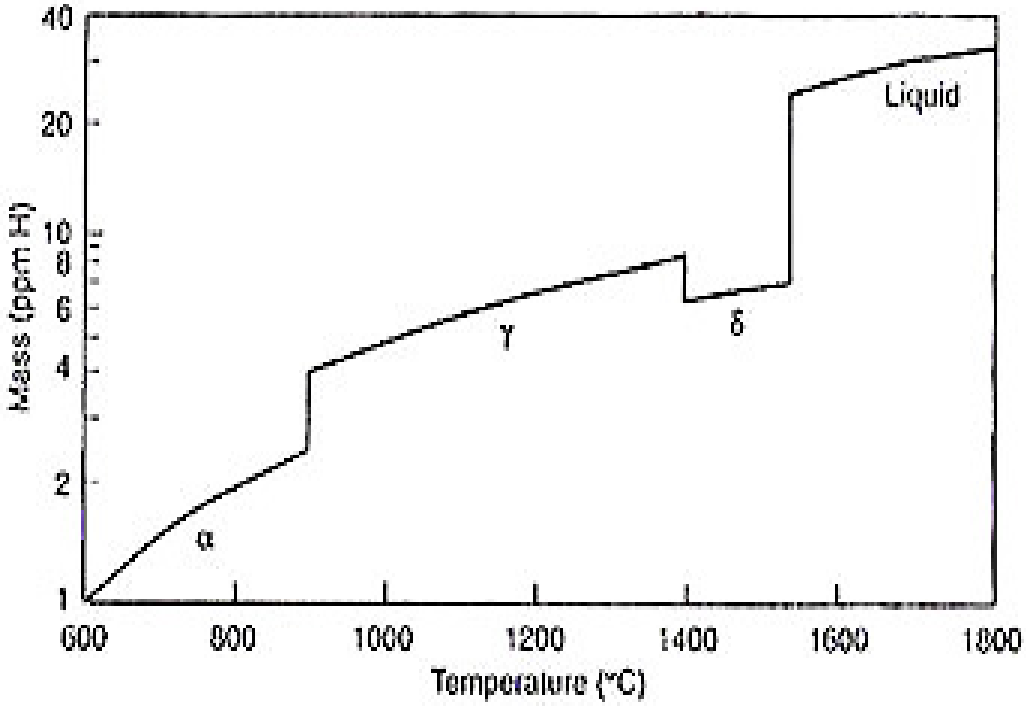

Figure 6: Solubility of hydrogen in pure iron at 1 atm pressure of H_2

In a permeation test with high purity iron, at steady state, the concentration of diffusible hydrogen was calculated using the fugacity, f = 10 MPa from a gas phase. The result obtained is 6.8×10^{-4} cm^3 H_2/100 g Fe, meaning one hydrogen atom occurs per approximately 3×10^7 Fe atoms, which is in agreement with the solubility of hydrogen at 293 °K [19].

In commercial grade iron and steel, under electrolytic charging, the total volume v_c of hydrogen taken up can attain tens or hundreds of cm^3 H_2/ 100 g Fe. From various literatures, these facts can be deduced: the saturation of a metal with hydrogen increases as, the pH of the electrolyte is lowered, the addition of hydrogen entry promoters, the higher the densities of the cathodic polarization current, higher degrees of cold plastic deformation of the metal and lower thickness of the specimen. Note that it is only a part of the hydrogen taken up by the commercial grade iron is available in solid solution, the rest of the hydrogen, v_c - c, is segregated at the dislocations and is precipitated in molecular form in micro-cracks and voids [19].

3.3.1 Interaction of hydrogen with the stress field

It is a known fact from thermodynamic that in metal, within the elastic region tensile stress decreases the chemical potential of hydrogen, whereas compression stress increases the chemical potential of hydrogen. Meaning that, tensile stress increases hydrogen solubility while compression stress is vice versa [19]. This increase is by elastic interaction of hydrogen with the stress field, caused by increase in tensile stress or higher hydrogen solubility, leading to increase in diffusivity of hydrogen. The solubility of hydrogen in iron is very low under room temperature and most hydrogen in steel are in trapped state at various defects, either reversibly or irreversibly. At equilibrium between solute hydrogen with trapped hydrogen, alternating stress is likely to change the solute concentration and induce trapping and detrapping of hydrogen with defects. As a result the defect acting as hydrogen traps would suffer alterations [20].

At equilibrium the relationship between hydrogen concentration and hydrostatic component of tensile stress is given as

$$c_\sigma = c_o \exp\left(\frac{\sigma V_H}{3RT}\right) \text{ or } \quad c_\sigma = c_o \exp\left(\frac{w}{Kt}\right) \tag{5}$$

Where c_σ, is hydrogen concentration in the region where the hydrostatic component of the tensile stress exist, σ is operative, c_o is the hydrogen concentration where σ = 0, K is the Boltzmann constant, w is the bonding energy of hydrogen with dislocations, V_H is the partial molar volume of hydrogen concentration in the metal obtained by measuring the rise or fall of the rate of hydrogen permeation through cathodically polarized membranes, at a constant overpotential, which were subjected to tensile or compressive stresses. The equation above also applies equally to stresses at the surface cracks and defects, as well as to internal stresses associated with dislocations and inclusions. With a large ratio of $\frac{w}{T}$ in the case of dislocation core the inadequacy of the equation was made obvious.

At the dislocations cores, which is a major player in the segregation of the interstitial atoms dissolved in iron, Fermi-Dirac statistics should be used, so that instead of the above equation, this is used.

$$\frac{c_d}{1-c_d} = \frac{c_o}{1-c_o} \exp\left(\frac{w}{RT}\right) \tag{6}$$

Where c_d and c_o are the equilibrium atom fractions of solute at dislocations and in free lattice sites, respectively, W is the bonding energy of hydrogen with dislocations. From this equation it can be seen that the distribution of hydrogen between the normal interstices and dislocations depends on the value of the bonding energy.

As higher stresses decreases the chemical potentials around its zone, hydrogen diffuses preferentially down the gradient to these locations, accumulating within this region [25]. The

figure below illustrates the various processes occurring in a fracture process zone (FPZ) ahead of the crack tip. FPZ is the region where hydrostatic stress is maximum. In addition to enhanced diffusion and trapping, by dislocations and inclusions, of lattice hydrogen to this region, re-distribution of hydrogen can also occur under the influence of a stress gradient.

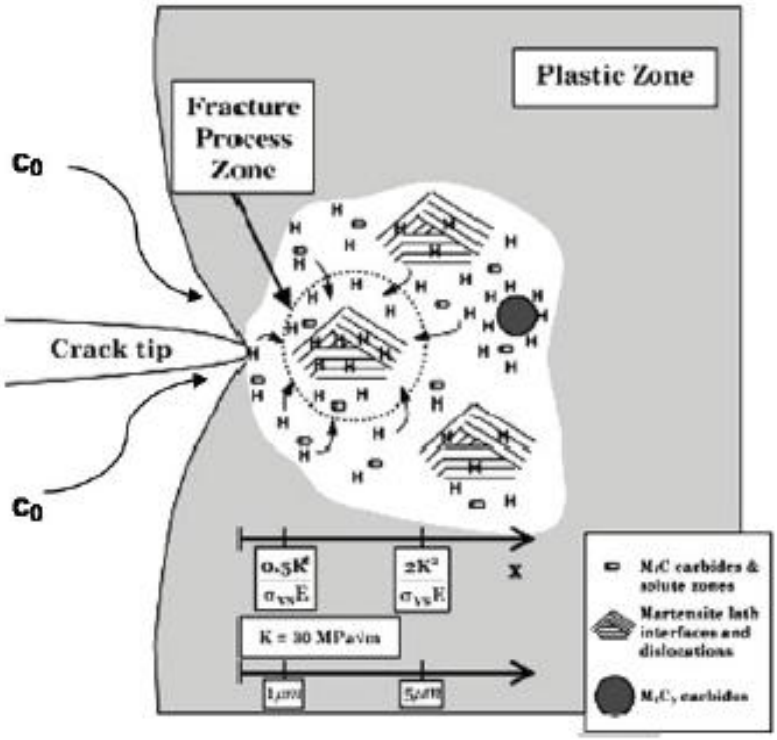

Figure 7: Schematic illustration of the processes occurring in the fracture process zone [25]

Solute adsorption fields: The interaction energy between solute atoms and the dislocation in the isotropic elastic for an edge dislocation is approximately given for an FCC metal and for a BCC metal respectively, as

$$W = A\sin\theta/r \quad \text{and} \quad W = \sigma_{ij}\epsilon_{ij}v \tag{7}$$

Where θ and r are cylindrical coordinates fixed on the dislocation and A is a parameter, containing positive independent material constants, σ_{ij} is the stress tensor of the dislocation, ϵ_{ij} is the local internal strain field produced by the solute atom referred to this reference volume and v is the reference volume containing the solute atom.

In screw dislocation, the stress field is in the coordinates fixed with X_3, parallel to the dislocation line.

3.3.2 Hydrogen trapping

Hydrogen absorbed by iron and steel may exist in different forms, namely

- Interstitial hydrogen, dissolved in the matrix of the solid solution
- Hydrogen associated with structural defects, such as dislocations
- Hydrogen accumulated at the voids or blisters in gaseous form

These different forms of hydrogen exhibit different mobilities which affects the mechanical and physical properties of the material to various degrees. The amount of interstitial hydrogen present in a material is a function of the charging conditions, i.e. the external environment, while the amount of hydrogen associated with dislocations and those accumulated in voids, tissues, etc, are functions of the composition and properties of the material [25].

Interstitial hydrogen, usually called lattice hydrogen, dilates iron crystal lattice. This occurs because the free space available at the interstitial site is smaller compare to the size of hydrogen. The extent of this dilation, which equals to the degree of strain field, can be obtained by the partial molar volume of hydrogen, V_H. V_H is reported for pure iron and Armco as 2.0 cm^3 mol^{-1} and 2.6 cm^3 mol^{-1} respectively using equation 5.

Hydrogen is a very reactive element. It interacts with any defects causing distortion on the lattice, e.g. dislocations, etc. As these defects dilate the iron lattice field causing distortions, hydrogen is attracted to the site. These sites called hydrogen trapping sites are characterized by different binding energies leading to reversible and irreversible trapping sites [25]. Trap sites, in the form of dislocations, can be introduced by cold work, particles and non-metallic inclusions. Generally trap sites decreases the apparent hydrogen diffusivity of iron and steel.

The concept of trapping originated as a result of attempts to understand the decrease of diffusivity of hydrogen in steels as a result of plastic deformation [27]. Hydrogen trapping is a phenomenon where various microstructural features in iron and steel have an attractive interaction with hydrogen. Such an interaction is originated by the energetically favorable condition for hydrogen to reside in the trap sites rather than in the lattice sites. At these trap sites hydrogen atoms spend more time than it would at normal lattice sites because the activation energy for escape from a tight binding site will be increased by the binding energy. Assuming that the metal contains a uniformly distributed population of traps, having different capacities of holding and delaying hydrogen atoms. In relation to their holding strength, traps can be classified at steady state as follows [7]:

1) **Reversible trap;** are traps in which the amount of trapped hydrogen is in equilibrium with those in diffusion process (lattice hydrogen). These are trap sites with lower binding energy. The amount of hydrogen concentrations in reversible traps is usually greater than

the concentration of hydrogen in lattice sites, because the residence time in reversible trapping sites are larger, examples can be found on table 2.

2) **Irreversible trap;** are traps with concentration of hydrogen atoms that are independent of those in diffusion process (lattice hydrogen) through the metal. These are trap sites with higher binding energy. Hydrogen in an irreversible trap can be removed from the diffusion process over a period of time depending on the temperature.

Also, hydrogen can react with itself to form H_2. H_2 as a gas exert the same pressure, such that if constrained in voids or micro-cracks, exerts significant pressure on the material. The total hydrogen concentration, in the absent of voids or micro-cracks, in the steel, C_T is given as the sum of the concentrations of lattice hydrogen, C_L and trapped hydrogen

$$C_T = C_L + c_r + c_i \tag{8}$$

Where c_r and c_i are the reversible and irreversible trapped hydrogen concentration. Note that c_r can contribute to diffusion of hydrogen in the lattice, so that C_r + C_L is called diffusible hydrogen.

Traps can provide a reservoir of hydrogen that can repartition to the region of highest hydrostatic stress at the crack tip, thereby decreasing the effective diffusivity and increasing the total hydrogen concentration. It also creates additional trap sites under the influence of self induced or external stress.

This total hydrogen partitioning can be calculated from thermodynamic principles as can be seen in equilibrium fractional hydrogen occupation at the trap sites or hydrogen concentration at the trap sites. The equilibrium between lattice and trap hydrogen atoms, with each one occupying a fraction θ_i, of the available sites, can be obtained by the equilibrium constant.

$$K = \frac{a_x}{a_L}, \tag{9}$$

Where a_L and a_x are the hydrogen activities on the lattice and trap sites respectively. At low lattice hydrogen concentration C_L, and low lattice fraction occupied θ_L, (C_L,$\theta_L \ll 1$) the equilibrium constant can be expressed as:

$$K = \frac{1}{\theta_L}\left(\frac{\theta_x}{1-\theta_x}\right). \tag{10}$$

Where $\theta_L \; and \; \theta_x$ are the fraction occupied sites for lattice and trap, respectively. Therefore the volume concentration of hydrogen within the two states of binding can be expressed as $C_L = N_L\theta_L$ and $C_x = N_x\theta_x$

Where N_L and N_x are number of lattice sites and trapped sites respectively [8].

The energy required to remove hydrogen which is called binding energy can be determined using thermal desorption spectroscopy (TDS). When the activation barrier to overcome the trap is small, traps of lower energy may reversibly trap hydrogen, depending on the temperature of the system, while deeper or stronger trap sites will irreversibly trap hydrogen, which can only be released at higher temperatures. The table 2 shows the number of traps types, their characteristic binding energies, their typical densities and whether they act as reversible or irreversible trapping sites.

Table 2: Characteristics of trap sites in iron and steel [25]

Trap type	Binding energy (E_B/kJ·mol^{-1})	Trap density (cm^{-3})	Degree of reversibility
Perfect lattice	0	8.5×10^{22}	-
Elastic dislocation**	20.2·(b/r)	4×10^{14} to 4×10^{20}	Reversible
H_2 vapour phase or in void	28.6	Dependent on steel properties	-
Dislocation core (screw)	20-30	10^{13} to 10^{19}	Reversible
Dislocation core (mixed)	58.6	4×10^{13} to 4×10^{19}	-
Grain boundary	~58.6	10^{13} to 10^{17}	Reversible/ irreversible
AlN particle interface	65	5×10^{18}	-
Free surface	70.7	10^{15}	-
Fe_3C interface	≥84	5×10^{18}	Irreversible
TiC interface	94.6	5×10^{18}	Irreversible
Roughened free surface	95.5	10^{15}	Irreversible

* Reference state is H in a perfect lattice
** Binding energy is inversely proportional to the distance from the dislocation, **b** is Burgers vector

3.3.3 Effect of material properties

The study of the material properties, such as chemical composition, microstructure, processed history and strength level are important to understand their influence on the diffusivity of hydrogen. To this effect, the activities of the individual components of typical steel are examined.

Carbon (C): carbon can exist in the steel as either lamellae pearlite or spheroidized carbides, the former when in nano-metric scale are uniformly dispersed and coherent with the matrix, acts as innocuous traps for hydrogen [24].

Manganese (Mn): The contributions and effects of Mn is rather complex. Mn is the main alloying elements in most of steels. It improves the strength and toughness of the steel by refining the microstructure. When present in the steel as MnS inclusion, it initiates sites for cracking. This initiation plays a critical role in the severity of trapping, depending on the shape of the inclusion. As elongated inclusions, the severity of trapping is high compared to when present as spherical inclusions. It has a high probability to segregate with other alloying elements and impurities [24, 25].

Chromium (Cr): The addition of up to 0.5% Cr to carbon steel decreases the rate of hydrogen permeation. A higher amount of Cr, in addition to Molybdenum and Nickel increases the susceptibility of the steel to HIC [24].

Copper (Cu): In amounts greater than 0.2% reduces hydrogen absorption from sulfide corrosion in intermediate pH environments (4.8-5.2) [24].

Sulphur (S): Sulphur is known as one of the most detrimental elements for HIC, especially when present in the material with elongated manganese sulfides structure. To evaluate the effect of sulphur, the amount of sulfides inclusions present and their shapes are significant factors to consider. When the inclusions are narrow, long and with sharp tips, they behave as internal cracks [24]. Figure 8, is a typical fracture surface of AISI 4340 steel in the presence of hydrogen sulfide. IG is the intergranular separation along prior austenite grain boundaries, QC is the quasi-cleavage and SC is the secondary cracking.

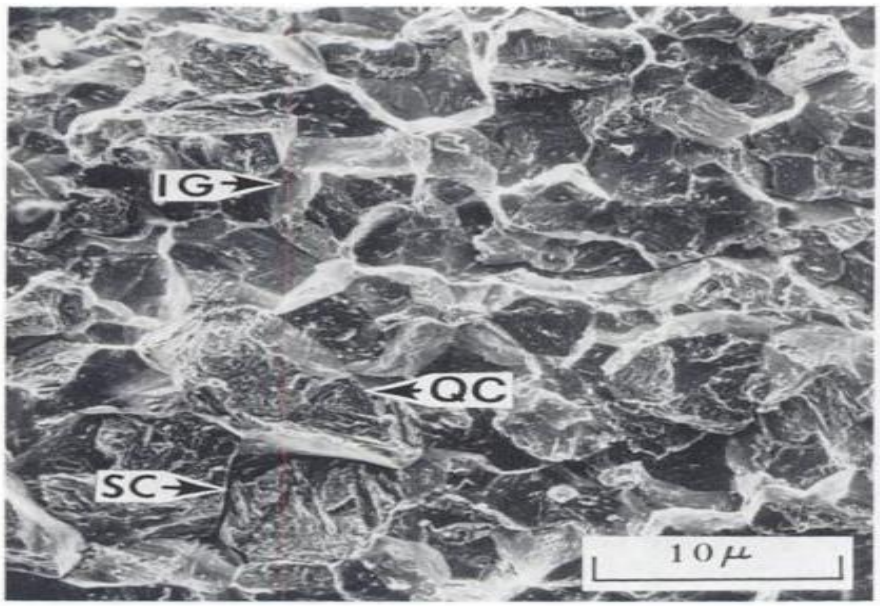

Figure 8: Scanning electron microfractograph of a fracture surface produced by crack growth in hydrogen sulfide

Phosphorus (P): P and similar elements such as S and Sb, segregates at the grain boundaries, increasing the crack growth susceptibility. P has been found to greatly affect the HIC in various low and high alloy steels. The effect of phosphorus concentration within the range of 0.005 to 0.17 %wt. on trapping of hydrogen at grain boundaries in low carbon steel, using thermal analysis technique, was reported by Jai-Young Lee. His conclusion was that the concentration of hydrogen trapped at grain boundaries decreases as the bulk phosphorus concentration increases and that tempering increases the phosphorus concentration [23].

Molybdenum (Mo) : Most steels are strengthen by quenching and tempering, which leads to high strength of the martensite, with a microstructure that is characterized by a high density of dislocations and high internal stresses, exactly the conditions that promote enhanced diffusion of hydrogen into the steel. On the other hand, Mo is used to achieve this same strength of steel without exposing the steel to an increase in diffusion of hydrogen, by solid solution strengthening and the formation of complex carbides together with other elements such as chromium and niobium [26].

Titanium (Ti), Niobium (Nb), and Vanadium (V): These are carbide and carbo-nitide precipitate formers in steel. The precipitates they form are usually smaller than 0.1 μm and homogeneously dispersed in the matrix such that they form active hydrogen trapping sites with high bonding energy.

On the other hand, the microstructure influences the trapping characteristics of the steel. Studies have shown that various microstructures produced by thermo-mechanical controlled processes (TMCP) on X-65 grade pipeline steel (0.05 wt% C, 0.002 wt% S) have different trapping efficiencies. These efficiencies were stated to increase in order as designated, pearlite $<$ ferrite/bainite $<$ acicular ferrite, accompanied by a total hydrogen concentration increasing by a factor of $\sim$2, with the effective diffusivity decreasing by the same proportion over the range of microstructures [42].

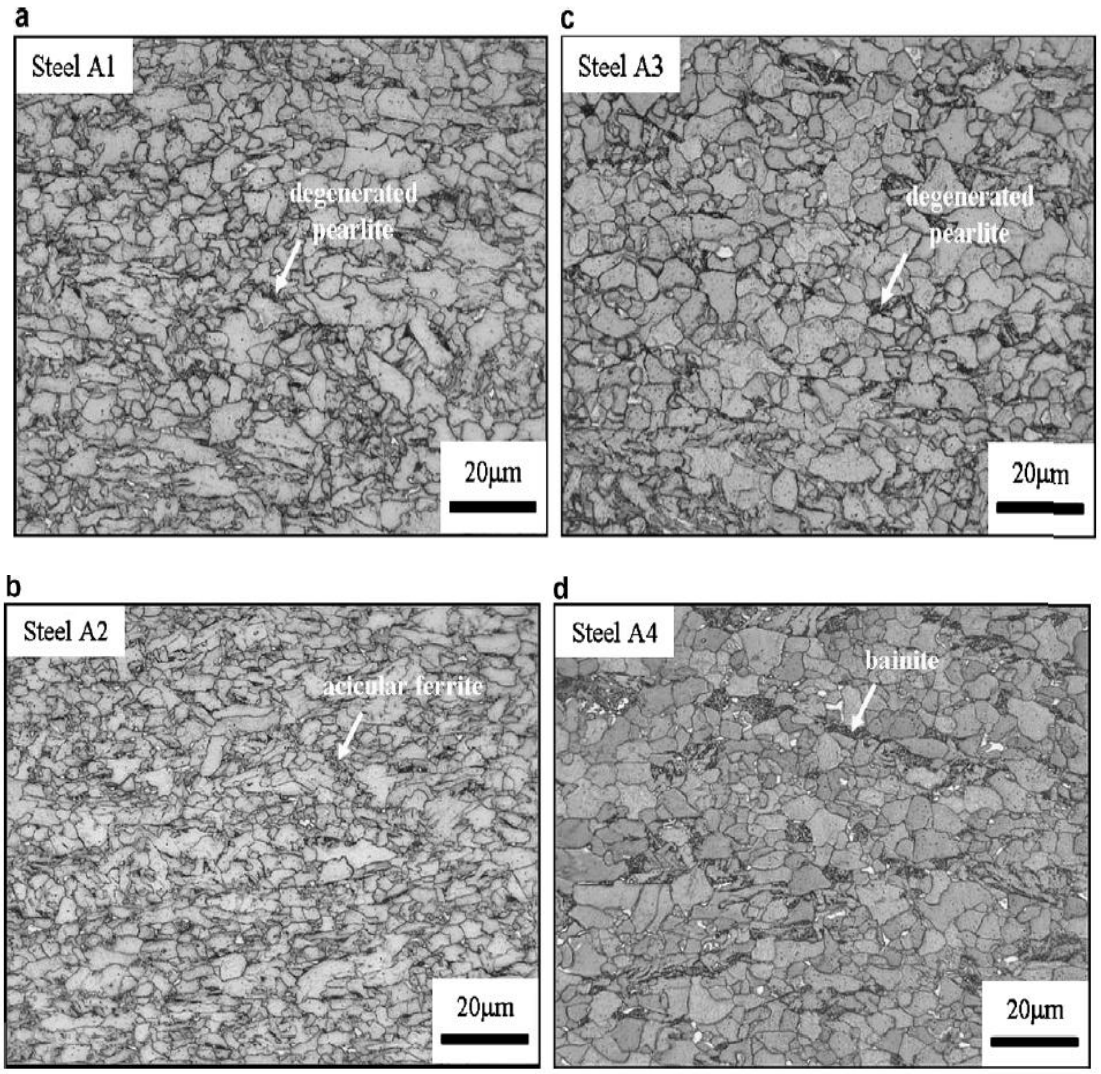

Figure 9: Optical microstructural image of X-65, showing degenerated pearlite, acicular ferrite, degenerated pearlite and bainite microstructures [42].

3.4 diffusion of hydrogen in a metal

Diffusivity of hydrogen in steel is a function of the crystal structure and it follows the Arrhenius equation:

$$D = D_0 \exp\left(-\frac{\Delta E}{RT}\right) \quad (11)$$

Where D is diffusivity, D_0 is a constant and ΔE is the activation energy for diffusion.

3.4.1 Effect of environment

The result of the measurements of hydrogen diffusivities at various temperatures found in literatures in general agrees with the above equations. These agreements follow from

$$D_0 = (\frac{1}{6}) a^2 f_d \exp(\frac{\Delta s}{R}) \quad (12)$$

From the theory of a body centered cubic lattice. Where a is the lattice parameter, f_d is the oscillation frequency of an impurity atom about its equilibrium position and Δs is the activation entropy. For instance if Δs = 0, then D_0 = 1.6 × 10^{-7} m^2 s^{-1} hydrogen in iron, but at high temperatures, hydrogen diffusion values are in the range of 3 × 10^{-8} to 2.2 × 10^{-7} m^2 s^{-1} [19].

3.4.2 Lattice diffusion

Lattice diffusion refers to the atomic diffusion within the crystalline lattice. Hydrogen diffusion within the crystal lattice occurs by interstitial.

For an ideal homogenous material (without traps) the depth of the potential wells and energy barriers between adjacent tetrahedral sites will be uniform. The diffusion D of such a medium is constant and the rate of transfer of hydrogen atoms is described by Fick's first law, while the distribution of hydrogen atoms in the steel can be derived from the solution of Fick's second law [6].

In the measurement of this flux, which can be either mass flux or molar flux, steady state or transient condition must be taken into account in the analysis of an electrochemical process. In general, the conditions for steady state $(\frac{\delta C}{\delta t} = 0)$ and for transient state $(\frac{\delta C}{\delta t} \neq 0)$ are governed by Fick's laws of diffusion. When molar flux and concentration rate strongly depend on the concentration gradient along the X-direction only and the diffusion flow is perpendicular to the moving plane of the solute.

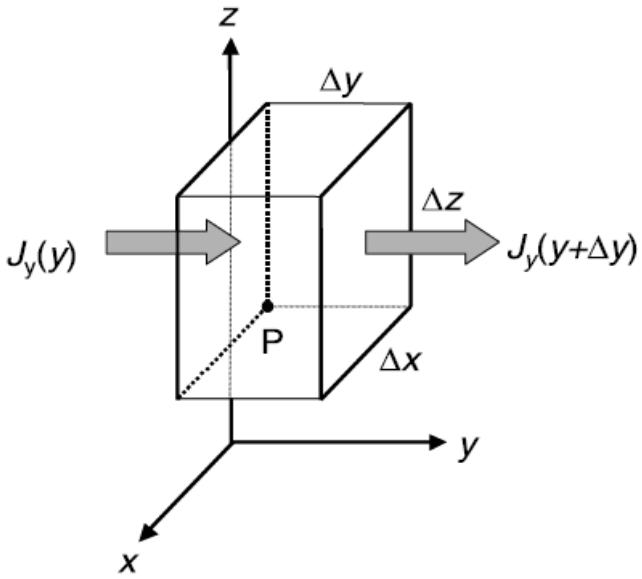

Figure 10: 3-dimentional stress distribution on a steel specimen [13]

These forms of Fick's first and second laws are applicable.

$$j_x = -D\frac{\delta C}{\delta x} \qquad \text{(Fick's First Law)} \qquad (13)$$

Fick's second law is a combination of first Fick's law and the continuity equation.

$$\left\{-\left[\frac{dJ_x}{d_x}+\frac{dJ_y}{d_y}+\frac{dJ_z}{d_z}\right]\Delta x\Delta y\Delta z=\frac{dC}{dt}\Delta x\Delta y\Delta z\right\}+\{-\nabla.J=\frac{dC}{dt}\} \qquad (14)$$

In one dimension

$$\frac{\partial c}{\partial t} = D\frac{\partial^2 c}{\partial x^2} \qquad \text{(Fick's Second Law)} \qquad (15)$$

Where j is the flux, c is the concentration of hydrogen, L is the thickness of the specimen and D is the diffusivity [13].

The solution of Fick's second equation depends on the system geometry which establishes a set of boundary conditions. The solution below is a particular case for semi infinite medium, under these conditions:

$C = C_0\ at\ X = 0\ and\ C = 0\ at\ X = \infty$ with the relation between $C\ and\ C_0$ give as

$$C = C_0 \text{erf}\left(\frac{x}{2\sqrt{Dt}}\right) \quad (16)$$

Take this into consideration, being $X_L = \infty$, steady state condition can not be reached at all.

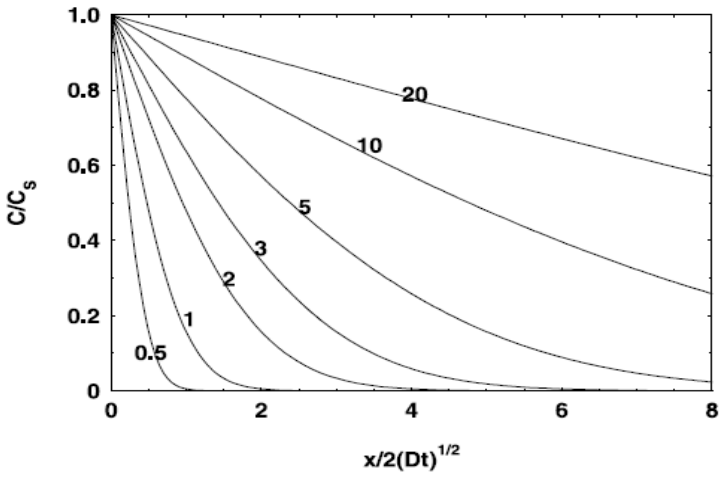

Figure 11: Solution of second Fick's law for the semi infinite condition ($X_L = \infty$)

If D is a constant, then the function y = f(X, t), can be define as

$$y = \frac{x}{2\sqrt{Dt}}, \quad \frac{dy}{dx} = \frac{1}{2\sqrt{\Delta t}} \quad \text{and} \quad \frac{dy}{dt} = \frac{-x}{4\sqrt{Dt}} \quad (17)$$

$$\frac{dc}{dt} = \quad \frac{dc}{dy}\frac{dy}{dt} = \quad \frac{-x}{4\sqrt{Dt^3}}\frac{dc}{dy} \quad (18)$$

$$\frac{d^2c}{dx^2} = \quad \frac{d}{dx}\left[\frac{dc}{dy}\left(\frac{dy}{dx}\right)\right] = \quad \frac{1}{4Dt}\frac{d^2c}{dy^2} \quad (19)$$

Substituting equation 19 and 20 into equation 16.

$\frac{dc}{dy} = \frac{-\sqrt{Dt}}{x}\frac{d^2c}{dy^2}$ z $\frac{1}{2y}$ $\frac{dz}{dy}$ such that $z = -\frac{1}{2y}\frac{dz}{dy}$ $-2\int y dy = \int \frac{dz}{z}$

Then $-y^2 = In\, z - In\, B$ (20)

Where B is the integration constant. Therefore:

$$z = Bexp(-y^2) \quad \text{and} \quad \int dc = B\int \exp(-y^2)\, dy \quad (21)$$

The function $f = \exp(-y^2)$ is responsible for the bell-shaped curve.

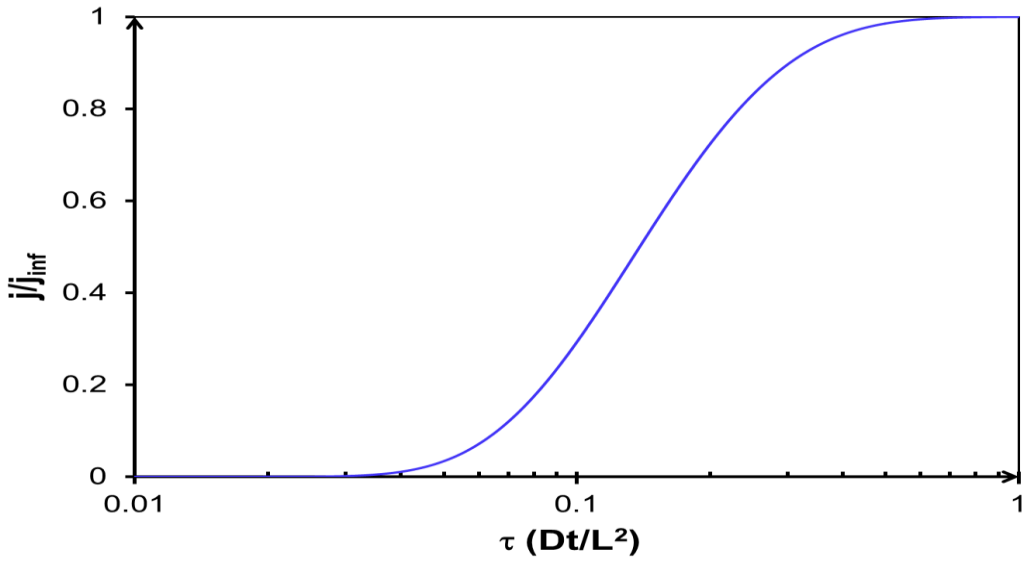

Figure 12: the bell shaped curve of a permeation test.

For a case of a finite thickness medium, the solution is given by the following

Still along the X-direction, if the concentration of hydrogen atoms at the charging (Input) cell is constant, an indication of attainment of equilibrium between the surface and the sub-surface coverage of hydrogen atoms which occurs instantaneously, and the concentration is zero at the oxidizing (output) cell, the permeation transient can be described by the Laplace and Fourier transformation under a given condition:

$$\frac{j_\tau}{j_\infty} = \frac{2}{\pi\tau^{0.5}} \sum_{n=0}^{\infty} \exp\left\{\frac{-(2n+1)^2}{4\tau}\right\} \quad \text{(Laplace Equation)} \qquad (22)$$

$$\frac{j_\tau}{j_\infty} = 1 + 2\sum_{n=1}^{\infty}\{(-1)^n \exp(-n^2\pi^2\tau)\} \qquad \text{(Fourier Equation)} \qquad (23)$$

Where j_∞ is the hydrogen flux at steady state, π is pie, j_τ / j_∞ is the normalized hydrogen flux as a function of the dimensionless time parameter $\tau = D.t / L^2$, as shown in figure 12, where t is time and L is the thickness of the membrane. Both equations give an equivalent result provided enough steps are allowed in the summation used [5].

If the boundary condition on the input side of the membrane is a constant flux, making the desorption step very slow. The flux is normalized by:

$$\frac{J_\tau}{J_\infty} = 1 - \frac{4}{\pi}\sum_{n=0}^{\infty}\frac{(-1)^n}{(2n+1)}\exp\{-\frac{(2n+1)^2\pi^2\tau}{4}\} \quad (24)$$

At steady state, if the charging current is removed, the transient follows decay. With a decay transient, the trapping sites in a material can be analyzed. Solving the decay of the permeation current from steady state for two limiting conditions is given by

A) The sub-surface concentration on the input side immediately goes to zero (fast decay), the normalized flux is given by:

$$\frac{J_\tau}{J_\infty} = 1 - \frac{2}{\pi^{1/2}}\cdot\frac{1}{\tau^{1/2}}\sum_{n=0}^{\infty}\exp\{-(2n+1)^{2/4\tau} \quad (25)$$

B) The flux across the input boundary is reduced to zero as soon as the charging current is switched off, here the hydrogen is exiting only from the anodic side (slow decay), the normalized flux is given by:

$$\frac{J_\tau}{J_\infty} = 1 - 2\sum_{n=0}(-1)^n erfc\frac{(2n+1)}{2\tau^{1/2}} \quad (26)$$

3.4.3 Diffusion with Traps

Contrary to a homogeneous material, in real materials, the depth of the potential wells and the height of the energy barriers are not uniform throughout the lattice due to the existence of grain boundaries, inclusions, dislocations and impurities. These sites can act as traps for hydrogen atoms because of deepening of the associated potential well. With these trapping sites acting as sinks for hydrogen atoms, Fick's second law is no longer valid. A valid equation for this situation should consist of a complete description of all the types of traps present in the different sites, the number of such site per unit volume and their average time of transfer between sites for each type of site. Leblond and Dubois [34], who reported the most comprehensive approach based on statistics of diffusion, taking into account all the requirements as list above, said that there were too many unknown parameters for practical application of their generalized equation. A more applicable equation was obtained by making the various assumptions discussed later in the chapter.

Alpha-ferrite (BCC microstructure) shows a hydrogen diffusivity of 1.6×10^{-9} m^2 s^{-1} at 25°c, austenite (FCC) shows a hydrogen diffusivity of 5.4×10^{-14} m^2 s^{-1}, which is about 4 to 5 orders lower and steel (BCC), a mixture of α-Fe and Fe_3C, shows a hydrogen diffusivity of 3×10^{-11} m^2 s^{-1}. Apart from composition as shown above, D also varies with the activation energy e.g. the diffusivity of α-Fe is 1.5×10^{-9} m^2 s^{-1}, 3.5×10^{-9} m^2 s^{-1}, and 6.7×10^{-9} m^2 s^{-1} at temperatures of

20°C, 100°C and 200°C, respectively, which is equivalent to the activation energy of 9.6 KJ mol^{-1}. Hydrogen diffusivity (lattice) D_L, can be related to apparent hydrogen diffusivity D_{app}:

$$D_{app} = D_L \frac{C_L}{C_L + C_x(1-\theta_x)}. \quad (27)$$

Where C_L is the lattice hydrogen concentration, C_x is the trapped hydrogen concentration and θ_x is the fractional occupation of trapping sites [8].

3.4.4 Permeation Test

Hydrogen permeation, remains the most useful method of studying diffusion of hydrogen through the membrane. In particular the electrochemical hydrogen permeation technique developed by Devanathan-stachurski [30].

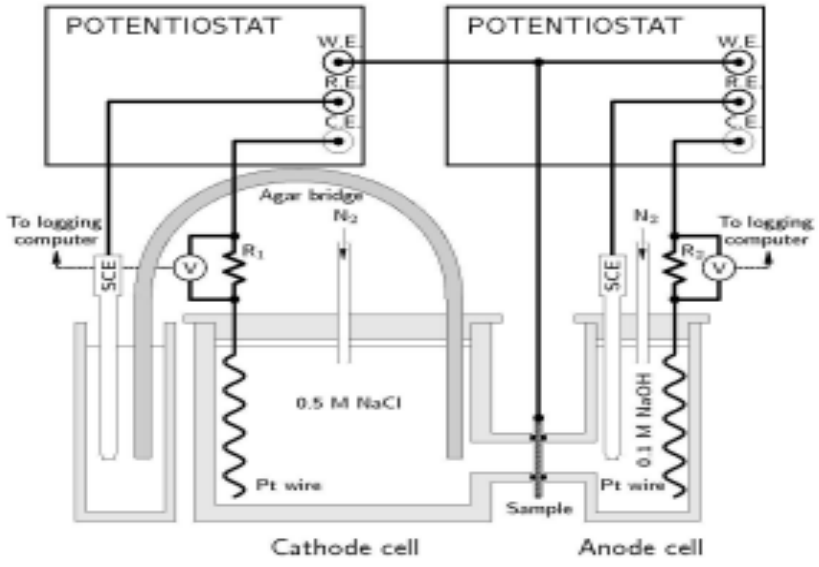

Figure 13: Schematic view of permeation cell

In this technique one side of the membrane is brough into contact with hydrogen source, for example by being cathodically polarized in the solution under study, whereas the other side is anodically polarized at constant potential in an alkaline solution to ionize the hydrogen emerging from the membrane. One must consider however to what extent the measured hydrogen flux through the membrane depends exclusively on the hydrogen entry process, because H permeation may be treated as being composed of three main stages: entry into the metal, diffusion through the membrane, exit of hydrogen from the metal. The mentioned stages may be characterized by the respective resistance:

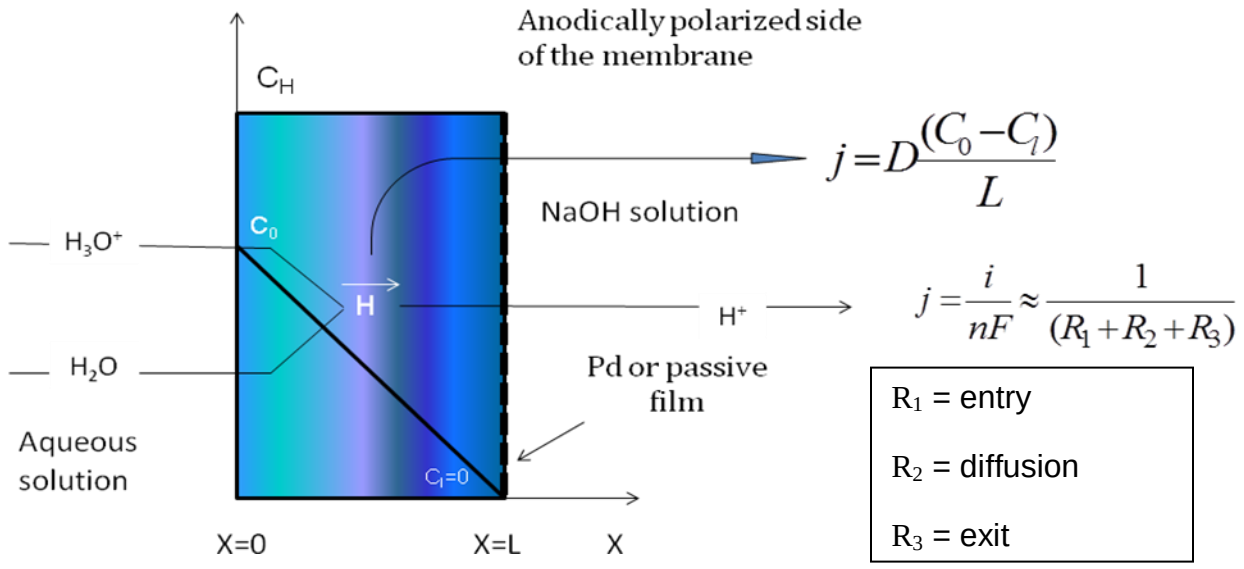

Figure 14: electrochemical methods for the study of hydrogen permeation.

in the case of iron or steel membrane, in order to accelerate the oxidation of hydrogen and to reduce the corrosion current of the exit side, this side is commonly coated with a thin palladium layer. If the suitable anodic potential is maintained, the whole of the hydrogen emerging from the membrane immediately undergoes ionization. Therefore the concentration of hydrogen just below the exit side C_L is zero and the hydrogen exit resistance can thus be disregarded. The diffusion resistance is defined by the ratio L/D (thickness to diffusivity). For a thin membrane this resistance may be small in comparison to hydrogen entry resistance, it means the permeation rate would be independent of the membrane thickness and is determined by the entry rate of hydrogen. If the thickness is large such that $R_2 > R_1$, the permeation rate is independent of entry rate.

The experimental procedure to obtain diffusion constant will be described in the next chapter. Here, it is worthwhile to note that several methods to calculate the diffusion constant have been reported in literature and we just want to take a look at some very important ones. Using the results obtained in hydrogen permeation test with palladium in a plot of anodic current against time as reported by Devanathan and Stachurski, the graph was obtained.

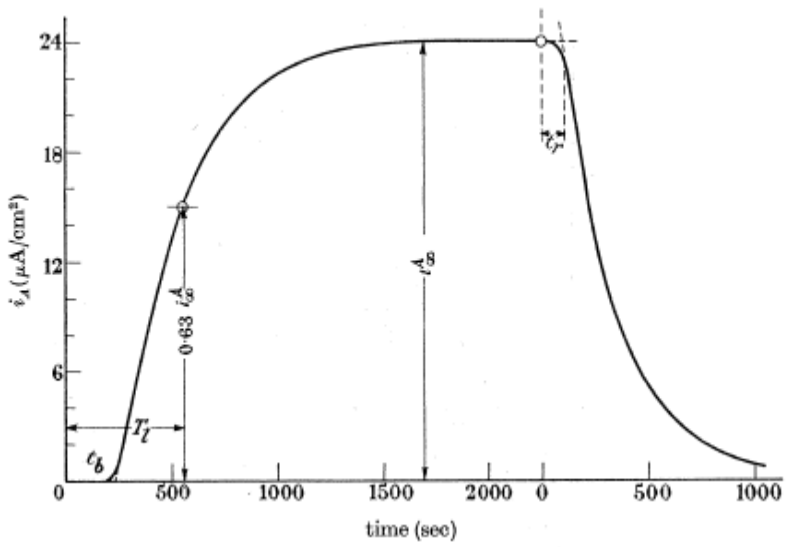

Figure 15: Typical permeation and decay transient record on contracted time scale

When such record of the instantaneous rate of permeation as this is available, the diffusion coefficient can be calculated by a variety of methods as follows:

1. ***The time lag method:*** This is achieved by integrating the rising curve to obtain the quantity of hydrogen which has permeated through the specimen at various times. Then extrapolating the plot of quantity against time gives the time lag, T_{lag} which is related to the diffusion constant by:

   $$T_{lag} = L^2/6D \qquad (28)$$

   Devanathan added, that the same value can be obtained by spotting the time at which the permeation is 0.6299 times of the steady state value. Values obtained from both method were in agreement
2. ***Rise time constant*** t_0***:*** The equation of the rising and decay transient respectively, which gives the same slop, is given by:

   $$In\left(\frac{P_b - P_\infty}{P_\infty}\right) = In\left[1 - e^{-3l/t_0} + e^{\frac{-8l}{t_0}} \ldots\right] + In2 - \frac{t}{t_0}$$ and $$In\left(\frac{P_t}{P_\infty}\right)$$ in both case for x = 0

   Of which t_0 is the rise time constant related to the diffusion constant by:

   $$t_0 = \frac{L^2}{\pi^2 D} \qquad (29)$$
3. **Breakthrough time** t_b method: The breakthrough time, is the difference of the corrected time lag plus the rise time constant t_0. Hence the diffusion constant is related to the breakthrough time by:

$$t_b = \frac{L^2}{D}\left(\frac{1}{6} - \frac{1}{\pi^2}\right) = \frac{L^2}{15.3D} \quad (30)$$

Permeation rate P: under diffusion theory conditions, permeation rate is related to the hydrogen coverage, θ by:

$$\frac{1}{P} = \frac{L_K^{b\to s}}{D\theta_K^{s\to b}} + \frac{2}{{}_K^{s\to b}\theta} \quad (31)$$

Where ${}_K^{s\to b} and {}^{b\to s}_K$ are the rate constants for the transfer of hydrogen from the surface to the bulk and vice versa. The above equation show a dependency of the reciprocal of permeation on thickness at constant D and θ. Although diffusion constant is independent of thickness of the specimen, at steady state, permeation rate could change irregularly if there is a change in the hydrogen coverage at the cathodic side of the membrane [30].

Results of measurements obtained in literature of apparent diffusivity of hydrogen in different steels and irons with different operating condition are summarized in table 3.

Table 3: Summary of the experimental conditions and results reported in literature

No	Material	Thickness (mm)	Temperature (° C)	Anodic electrolyte	Cathodic electrolyte	Anodic Voltage	Cathodic current density	Diffusivity 10^{-11} m^2 s^{-1}
[1]	Ferro Armco	-	22	NaOH 0,2 N	H_2SO_3 0,1 N e NaOH 0,2 N	-	Galvanostatic: 0,021 ÷ 4,3	416 ÷ 845
[2]	Ferro Armco	1	25	NaOH 0,1 M (Pd coating)	NaOH 0,1 M	+ 0,32 vs SHE	Galvanostatic: 10	130 ÷ 770
[4]	Ferro Armco	0,5 ÷ 1,6	25	NaOH 0,1 M (Pd coating)	0,5% CH_3COOH + 5% NaCl + H_2S	0 vs HgO/Hg	-	-
[9]	X56	0.75	25÷45	NaOH 0,1 M	NaOH 0,1 M	-	Galvanostatic: 2	18 ÷ 85
[21]	Pd	0,035 ÷0,54	25	NaOH 0,1 N	NaOH 0,1 N	- 0,3 vs SCE	Galvanostatic: 0,01	1 ÷ 2
[10]	X65	1	25	NaOH 0,1 M	$NaHCO_3$ 10^{-3} M + AQDS 10 ppm + Na_2S 10 ppm	+ 0,2 vs SCE	-	9 ÷ 10
[11]	Fe-C-Mo martensitic HSLA steel	1,1	10÷40	NaOH 0,1 M	H_2SO_4 1 M	-0,358 vs SSE	Galvanostatic: 5 ÷ 200	4 ÷ 8

[29]	Ferro Armco, zone refined(ZR) iron and AISI 4340	10	25	NaOH 0,1 N	NaOH 0,1 N e H_2SO_4 0,1 N	-	Galvanostatic: < 15	625 ÷ 825
[21]	Ferro Armco	0,77	25	NaOH 0.1 M	H_2SO_4 1 N	-	Galvanostatic: 0,4 ÷ 4,3	-
[32]	Carbon steel	0,85 ÷ 0,95	25	NaOH 0,1 N	H_2SO_4 0,9% + H_2SeO_3 2,5 ppm	- 0,45 vs SCE	Galvanostatic: 1	0.3 ÷ 9
[32]	Fe-Ni alloy	-	25	NaOH 0,1 M with Pd coating	H_2SO_4 1 N e NaOH 0,1 M	- 0,6 vs SCE	-	-
[33]	HSLA carbon	-	25	NaOH 0,1 M	NaCl 3,5%	+ 0,2 vs SCE	Potentiostat: -1,050 vs SCE	-
[34]	X65	0,5 ÷ 10	25÷55	NaOH 0,1 M	NaCl 5% e sodium acetate 0,4	+ 0,6 vs open circuit	-	-
[35]	Fe and carbon alloy	-	25	NaOH 0,1 M with Pd coating	NaOH 0,1 M con Pd coating	+ 0,2 vs SHE	-	1 ÷ 4
[36]	AISI 410 stainless steel	0.25	25	NaOH 0.1 M	NaCl 5% + CH_3COOH + H_2S	+ 0,3 vs SCE	Free corrosion potential	0.3 ÷ 3
[37]	Ferro Armco	0,5 ÷ 2	25	NaOH 0.1 M	NaOH 0.1 M	- 0.22 vs Hg/HgO	Galvanostatic: 2	1 ÷ 3.5
[38]	Fe – α	0.5 ÷ 1	25	NaOH 0.1 M	3.5 % NaCl + H_2S	+ 0.3 vs SCE	Galvanostatic: 1	720

It is also shown that $V_d = 0.33V_0$, for a unit surface of $V_0 = C_L / 2$, where V_d is the hydrogen evolved through the anodic surface and V_0 is the total quantity of diffusible hydrogen in the membrane. If for a trap free metal the numerical value of the coefficient, $\frac{V_d}{V_0} > 0.33$, it only means surface processes occurring on the cathodic polarization side is suppressing the desorption of hydrogen [19].

3.5 Mathematical Modeling of hydrogen diffusion

For the reiterating all that has been stated before now on the modeling of hydrogen diffusion through a medium, I would like to take them in their chronological order starting with McNabb and Foster.

3.5.1 McNabb and Foster [32]

They established the families of three kinds of trapping sites namely, interstitial (lattice) sites, reversible sites and irreversible sites, but assumed that irreversible trapping sites were already saturated by hydrogen and do not have any effects on the diffusion process, so were eliminated

from the model. McNabb and Foster obtained a general diffusion equation for hydrogen under the said conditions in a medium containing reversible traps as follows:

$$\frac{dc}{dt} + N\frac{dn}{dt} = \nabla.(D\Delta c) \tag{32}$$

For the simultaneous occurrence of trapping and releasing reaction, the equation is described by:

$$\frac{dn}{dt} = Kc(1-n) - pn \tag{33}$$

Where *C* is hydrogen concentration as a function of position and time *C (X, Y, Z, t)*, *N* is the density of reversible traps (number per unit volume), *n* is the occupied fraction, *P* is the probability of release of hydrogen in one second, by a reversible trap, *K* is the number of hydrogen atoms captured per seconds in a given volume *dV*.

Using the non-dimensional variables:

$$u = \frac{C}{C_0}, \quad \omega = nNC_0, \quad V = C_0K\frac{a^2}{D}, \quad \tau = D\frac{t}{a^2}, \quad \lambda = NK\frac{a^2}{D} \quad \text{and} \quad u = p\frac{a^2}{D}$$

The above equation becomes:

$$\frac{du}{d\tau} + \frac{d\omega}{d\tau} = \nabla^2 \mathrm{u} \tag{34}$$

$$\frac{d\omega}{d\tau} = \lambda u - u\omega - Vu\omega \tag{35}$$

The authors reported that in steady state, the ratio between the average hydrogen content, Q_0 in a membrane and the content with $C(X) = C_0(Q_1)$ is not half as in classical theory but $1/2 < Q_0/Q_1 < 1$. Stating that the ratio is $^1/_2$ *if* $K << p$, tends to maximum value between ½ and 1, if the ratio K/p increases and then decreases to ½ again, if $K >> p$.

Hydrogen flux through the surface s of the membrane is given by:

$$P(\tau) = \frac{C_0D}{a}\iint_s \frac{du}{dn}ds \tag{36}$$

For $\tau \to \infty$ the flux approaches a constant value, therefore it integral in time, which is the total quantity of hydrogen that will pass through the surface in time, τ tends to an asymptote. The intercept of the asymptote on the τ-axis is used in calculation of *D* as follows:

$$\tau_i = t_i\frac{D}{a^2} = \frac{1}{6} + \frac{\alpha}{2\beta} + \frac{\alpha}{\beta^2} - \frac{\alpha}{\beta^3}(1+\beta)\log(1+\beta) \tag{37}$$

$$\alpha = \frac{NK}{p} \quad \text{and} \quad \beta = \frac{C_0K}{p}$$

Alternatively to obtain *D* from previous equation, it is necessary to measure the values of the four parameters,: *N*, *K*, *p* and C_0 . For a case of a thick specimen and a low hydrogen concentration, apparent diffusion coefficient, D_{app} is related to the lattice diffusion coefficient by:

$$\frac{D_L}{D} = 1 + \frac{K}{p} N_T \tag{38}$$

3.5.2 Oriani: [8]

He established the availability of two types of sites for hydrogen occupancy, namely: Normal (lattice) sites characterized by normal enthalpy of solution and trapping sites, which provide an energetically favored environment for occupancy by the hydrogen. These two atomic populations occupies fractions, θ_i of the available sites and are in equilibrium with each other described by

$$K = \frac{a_x}{a_L} \tag{39}$$

Such that Fick's first law is given by:

$$J = -D_L dC_L / d_x$$

But for experimental purposes he used

$$J = -D_{app}\, dC_T / d_x$$

Such that the two diffusion coefficients are related by:

$$D_{app} = D_L (1 + (N_x N_L K)/(N_L + K C_L)^2)^{-2} \tag{40}$$

$$D_{app} = D_L \left(\frac{C_L}{C_L + C_x(1-\theta_x)}\right) \tag{41}$$

3.5.3 M. Lino [33]

In his description of hydrogen diffusion in a system with one kind of trap, he started with McNabb and Foster equation. Applying the same assumptions, except in the equation describing the simultaneous occurrence of trapping and releasing reaction, which he gave as:

$$\frac{d\theta}{dt} = KC(1-\theta) - p\theta \tag{42}$$

Where θ is the trap occupancy fraction. For a system of low hydrogen concentration, like in iron/H system, the equation becomes:

$$\frac{d\theta}{dt} = KC - p\theta \tag{43}$$

Analyzing for a slab of thickness, ɐ using the non-dimensional variables:

$$u = \frac{C}{C_0}; \quad V = N\frac{\theta}{C_0}; \quad \vartheta = \frac{x}{\mathfrak{e}}; \quad \tau = D\frac{t}{d^2}; \quad \lambda = NK\frac{a^2}{D}; \quad \mu = p\frac{a^2}{D}$$

$$\frac{du}{d\tau} + \frac{dV}{d\tau} = \frac{d^2u}{d\vartheta^2} \tag{44}$$

$$\frac{dV}{d\tau} = \lambda u - \mu V \tag{45}$$

With: u = V = 0 for $\tau < 0$

u = 0 at $\vartheta = 0$ for $\tau > 0$

u = 1 at $\vartheta = 1$ for $\tau > 0$

Such that the solution of the system is given as:

$$u = \vartheta + \sum_{n=1}^{\infty}(-1)^n \frac{2n\pi sinn\pi\vartheta}{s_n^-[1+\frac{\lambda\mu}{(s_n^- - \mu)^2}]} e^{-s_n^-\tau} + \sum_{n=1}^{\infty}(-1)^n \frac{2n\pi sinn\pi\vartheta}{s_n^+[1+\frac{\lambda\mu}{(s_n^+ - \mu)^2}]} e^{-s_n^+\tau} \tag{46}$$

With: $s_n^{\pm} = 1/2[\lambda + \mu + n^2\pi^2 \pm \sqrt{(\lambda + \mu + n^2\pi^2)^2 - 4\mu n^2\pi^2}]$ (47)

For a non-dimensional form, the permeation flux is given as:

$$j(0,\tau) = J(0,\tau)\frac{a}{DC_0} = (\frac{du}{d\vartheta})_{\vartheta=0} \tag{48}$$

Differentiating u with respect to ϑ and letting $\vartheta = 0$, a general equation for diffusive permeation through the exit surface of the membrane for a system with low hydrogen concentration and reversible traps is obtained as follows:

$$j(0,\tau) = 1 + \sum_{n=1}^{\infty}(-1)^n \frac{2n^2\pi^2}{s_n^-[1+\frac{\lambda\mu}{(s_n^- - \mu)^2}]} e^{-s_n^-\tau} + \sum_{n=1}^{\infty}(-1)^n \frac{2n^2\pi^2}{s_n^+[1+\frac{\lambda\mu}{(s_n^+ - \mu)^2}]} e^{-s_n^+\tau} \tag{49}$$

For a very low probability of hydrogen capture by traps $(K << 1)$, λ is negligible, substituting into the equations above:

$$u = \vartheta + 2\sum_{n=1}^{\infty}\frac{(-1)^n}{n\pi} sinn\pi\vartheta e^{-n^2\pi^2\tau} \tag{50}$$

$$j(0,\tau) = 1 + 2\sum_{n=1}^{\infty}(-1)^n e^{-n^2\pi^2\tau} \tag{51}$$

Which are in agreement with classical theory. The figure below shows a graphical representation of the relationship between λ and μ, for the case of $\lambda = 10$ and μ ranging from10^{-3} to 10^{3}.

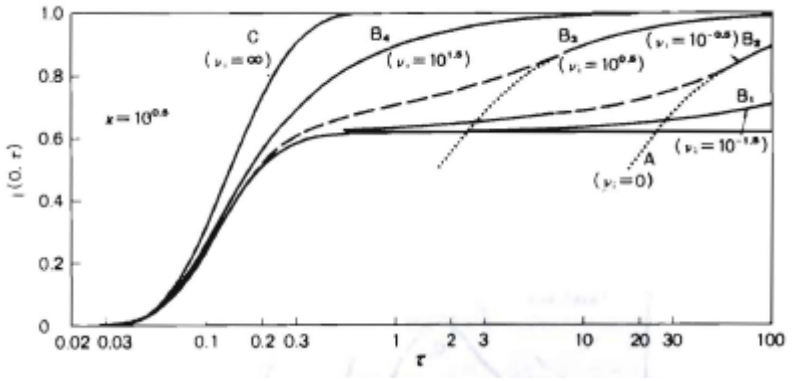

Figure 16: Normalized permeation transient in the presence of three types of sites (two types of traps)

Hydrogen diffusion in a system with irreversible traps: In this kind of system, the probability of hydrogen capture λ has a finite value, while the probability of hydrogen release μ has an infinitesimally small value. The equation for this system is obtained as follows:

$$u = \frac{sinh\sqrt{\lambda\vartheta}}{sinh\sqrt{\lambda}} + \sum_{n=1}^{\infty}(-1)^n \frac{2n\pi sinn\pi\vartheta}{\lambda+n^2\pi^2} e^{-(\lambda+n^2\pi^2)\tau} \quad (52)$$

$$j(0,\tau) = \frac{\sqrt{\lambda}}{sinh\sqrt{\lambda}} + \sum_{n=1}^{\infty}(-1)^n \frac{2n^2\pi^2}{\lambda+n^2\pi^2} e^{-(\lambda+n^2\pi^2)\tau} \quad (53)$$

Such that in a system with reversible traps, the steady state hydrogen distribution is given as:

$$u^{\infty} = \frac{sinh\sqrt{\lambda\vartheta}}{sinh\sqrt{\lambda}} \quad (54)$$

And the maximum permeation flux is given as:

$$j(0,\infty) = \frac{\sqrt{\lambda}}{sinh\sqrt{\lambda}} \quad (55)$$

Hydrogen diffusion in a system with both reversible and irreversible traps: A suitable equation for this type of system is given as follows:

$$\frac{du}{d\tau} + \frac{dV}{d\tau} + \frac{d\omega}{d\tau} = \frac{d^2u}{d\vartheta^2} \quad (56)$$

$$\frac{dV}{d\tau} = \lambda u - \mu V \quad (57)$$

$$\frac{d\omega}{d\tau} = ku(1-\theta_i) \tag{58}$$

Where $\omega = N_i \frac{\theta_i}{C_0}$ and $k = N_i K_i \frac{a^2}{D}$, and i is the irreversible traps. When irreversible traps in the system are far from being saturated($\theta << 1$), then $\frac{d\omega}{d\tau} = ku(1-\theta) \quad \rightarrow \quad \frac{d\omega}{d\tau} = u$k

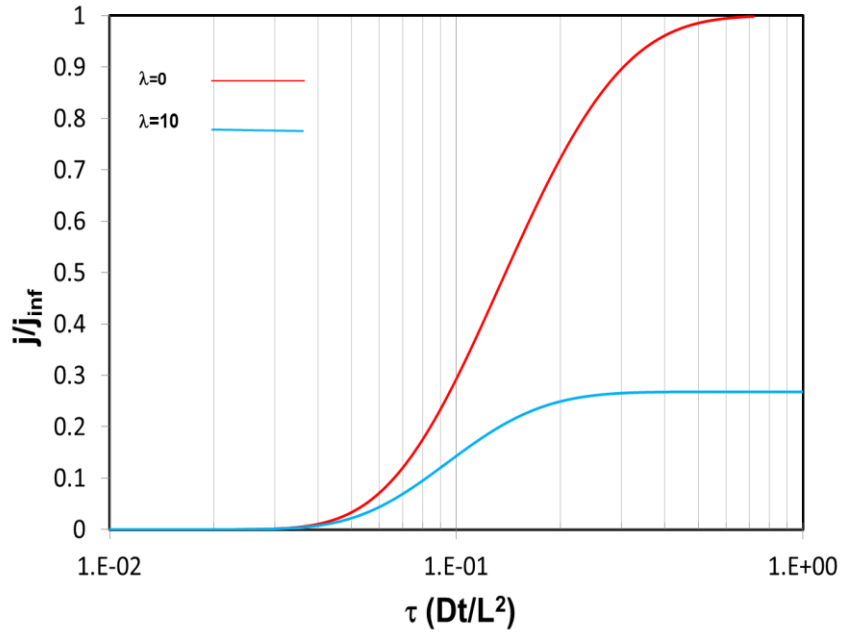

Figure 17: permeation transient in the presence of two types of sites (one type of trap, ir-reversible traps)

For initial boundary conditions as follows:

$$u = V = \omega = 0 \qquad for\ (\tau < 0)$$

$$u = V = \omega = 0 \qquad at\ \vartheta = 0 \qquad for\ (\tau > 0)$$

$$u = 1 \qquad at\ \vartheta = 1 \qquad for\ (\tau > 0)$$

Applying these boundary conditions to a system with irreversible traps is given by:

$$u = \frac{1}{s} . \frac{sinh\sqrt{k+s+\frac{\lambda s}{s+\mu}}\vartheta}{sinh\sqrt{k+s+\frac{\lambda s}{s+\mu}}} \tag{59}$$

$$u = sinh\frac{\sqrt{k}\vartheta}{sinh\sqrt{k}} + \sum_{n=1}^{\infty}(-1)^n \frac{2n\pi sinn\pi\vartheta}{s_n^-[1+\frac{\lambda\mu}{(s_n^- - \mu)^2}]} e^{-s_n^-\tau} + \sum_{n=1}^{\infty}(-1)^n \frac{2n\pi sinn\pi\vartheta}{s_n^+[1+\frac{\lambda\mu}{(s_n^+ - \mu)^2}]} e^{-s_n^+\tau} \tag{60}$$

$$s = -s_n^{\pm} = -1/2[n^2\pi^2 + k + \lambda + \mu \pm \sqrt{(k+\lambda+\mu+n^2\pi^2)^2 + 4\mu n^2\pi^2}] \tag{61}$$

Differentiating with respect to ϑ , and letting $\vartheta = 0$, the equation becomes:

$$j(0,\tau) = sinh\frac{\sqrt{k}}{sinh\sqrt{k}} + \sum_{n=1}^{\infty}(-1)^n \frac{2n^2\pi^2}{s_n^-[1+\frac{\lambda\mu}{(s_n^- - \mu)^2}]} e^{-s_n^-\tau} + \sum_{n=1}^{\infty}(-1)^n \frac{2n^2\pi^2}{s_n^+[1+\frac{\lambda\mu}{(s_n^+ - \mu)^2}]} e^{-s_n^+\tau} \quad (62)$$

***Influence of trapping on apparent hydrogen diffusivity*:** the total quantity of hydrogen that has passed from plane X = 0, at t = 0 to t = t, per unit area (Q) {apparent hydrogen diffusion constant}, can be calculated by

$$Q = C_0 a \int_0^{\tau} d\tau (\frac{du}{d\vartheta})_{\vartheta=0} \quad (63)$$

$$\bar{Q} = C_0 a . \frac{1}{s^2} . \frac{sinh\sqrt{k+s+\frac{\lambda s}{s+\mu}}}{sinh\sqrt{k+s+\frac{\lambda s}{s+\mu}}} \quad (64)$$

$$Q = C_0 a \frac{\sqrt{k}}{sinh\sqrt{k}}(\tau - L) + transient\ terms. \quad (65)$$

Where $L = \frac{1}{6}\left(1 + \frac{\lambda}{\mu}\right).\frac{3}{k}(\frac{\sqrt{k}}{sinh\sqrt{k}} - 1)$ (66)

In a plot of Q against time t, the slope of the asymptote is given by:

$$slope = \frac{\sqrt{k}}{sinh\sqrt{k}} . \frac{DC_0}{a} \quad (67)$$

The time lag is given by $time\ lag = \frac{a^2}{6D}\left(1 + \frac{\lambda}{\mu}\right).f(k)$ (68)

Note that $f(k) \approx 1 - \frac{k}{15} \to 1$

For a system with multiple traps with parameters $(\lambda_1, \mu_1), (\lambda_1, \mu_1), \ldots\ldots (\lambda_N, \mu_N)$ $and\ k_1, k_2, \ldots\ldots k_M$, the corresponding values of the slop is given by:

$$slope = \frac{\sqrt{\sum_{j=1}^{M} k_j}}{sinh\sqrt{\sum_{j=1}^{M} k_j}} . \frac{DC_0}{a} \quad (69)$$

And the corresponding value of time lag is given by:

$$time\ lag = \frac{a^2}{6D}\left(1 + \sum_{j=1}^{N}\frac{\lambda_j}{\mu_j}\right).f(\sum_{j=1}^{M} k_j) \quad (70)$$

Finding the integral solution of the covering rate of trap sites:

$$\frac{d\infty}{d\tau} = Vu(1-\theta) - \mu\theta \qquad and \qquad \frac{d\theta_i}{d\tau} = V_i u_i(1-\theta_i)$$

Where $\theta \;\; and \;\; \theta_i$ are related to $v \;\; and\, \mu$ as in

$$v = N\frac{\theta}{C_0}; \quad \mu = p\frac{a^2}{D}; \quad V = C_0 k\left(\frac{a^2}{D}\right) and \quad \omega = C_0 k_i(\frac{a^2}{D})$$

With initial conditions as $\theta(\vartheta,\tau) = 0 \quad for\, \tau = 0$

$$\theta = Vexp[-\int_0^{\tau} d\tau(\mu + Vu] \times \int_0^{\tau} d\tau\{uexp[\int_0^{\tau} d\tau(\mu + Vu]\} \qquad (71)$$

With initial conditions as $\theta_i(\vartheta,\tau) = 0 \quad for\, \tau = 0$

$$\theta_i = 1 - \exp(-V_i \int_0^{\tau} d\tau u) \qquad (72)$$

Such that, at the entry side, with boundary condition as $(1,\tau) = 1$, the equations become:

$$\theta(1,\tau) = \frac{V}{\mu+V}[1 - e^{-(\mu+V)\tau}] \qquad (73)$$

And $\theta_i(1,\tau) = 1 - e^{-V_i\tau}$ (74)

When $\frac{(\mu+V)D}{a^2} = p + C_0 k \quad or \quad V_i(\frac{D}{a^2})$ is small;

The initial stage diffusion theory of low coverage model can be successfully applied. Lino used experimental data to estimate the kinetics of reversible trap coverage $\approx \theta(1,\tau)$, and irreversible trap coverage$\approx \theta_i(1,\tau)$.

3.5.4 Leblond and Dubois [34]

They obtained a general equation of hydrogen diffusion in steel on the basis of statistical treatment of the random movement of hydrogen atoms.

They reported that the equation they generated for the general case of hydrogen diffusion depended on too many unknown function and physical parameters and that the physical interpretations of this different terms of the equation was not obvious. In order to proceed, they had to make some assumptions as listed below:

1) the probability of capture was the same for each type of site, meaning that the heights of the potential barriers is not dependent on the nature of the sites, but varies in each case, making it such that, there are no attracting or repelling sites

2) that the material contains three types of sites namely diffusion sites, reversible trap sites and irreversible trap sites. Such that all sites are considered collectively in the three categories with average times of transfer for each type

3) that the trap sites are essentially surrounded by normal diffusion sites, such that there are no direct path between the two trapping sites. Limitation of this assumption occurs in the case of rapid diffusion along preferential paths such as dislocations or grain boundaries. In these cases the height of the barriers exhibits some directionality.

With the assumptions they derive the equation as follows:

$$2D_{kl}\nabla In\Psi_l = 2D_k\nabla In\Psi = \frac{\nabla(D_k s_k)}{s_k} \quad (75)$$

Where s_k is the solubility of hydrogen at the pressure p_0 ,

On further application of mathematical treatment, they obtained this simplified equation:

$$\frac{dn_k}{dt} = -\frac{n_k}{\tau_k} + \sum_{l=1}^{m}\frac{p_l n_l}{\tau_l} + \sum_{l=1}^{m}\nabla[D_l s_l \nabla\left(\frac{p_l n_l}{s_l}\right)] \quad (76)$$

If A = $-\frac{n_k}{\tau_k} + \sum_{l=1}^{m}\frac{p_l n_l}{\tau_l}$ describing the local thermodynamic equilibrium between the sites. (77)

and B = $\sum_{l=1}^{m}\nabla[D_l s_l \nabla\left(\frac{p_l n_l}{s_l}\right)]$ is the diffusion term involving the gradients of the activity. (78)

Defining hydrogen permeability parameter (f) as $f = D_l s_l$

Such that the activity (A) $is\ given\ as$ $A = \sum_{l=1}^{m}\frac{p_l n_l}{s_l}$ (79)

With $\frac{1}{\tau_l} \cong \gamma D_l = \frac{\gamma f}{s_l}$

The finial equation is obtained as:

$$\frac{dn_k}{dt} = \gamma f\left[-\frac{n_k}{s_k} + A\right] + \nabla(f\nabla A) \quad (80)$$

3.6 Mathematical modeling of Hydrogen desorption

At interruption of the charging (cathodic) current, hydrogen atoms diffused from both the anodic and cathodic sides of the membrane. Ideally, in order to capture the total quantity of hydrogen dissolved out from the membrane, measurements are supposed to be taken from both sides, but due to the difficulties and the time laps during the change over from cathodic solution to NaOH in the cathodic compartment, most authors measures the desorption of hydrogen only from the anodic compartment. To this effect Zakroczymski, showed the relationship of measuring

hydrogen desorption from the two sides and how it is related the total hydrogen dissolved out of the membrane.

3.6.1 Zakroczymski [28]

A membrane with diffusible hydrogen only:

If initial conditions are: concentration in the membrane at entry side is constant (C_0), at the exit side it equals to zero ($C_L = 0$) and hydrogen diffusivity D = constant (steady state), such that hydrogen concentration drops linearly across the membrane

$$C = C_0(1 - \frac{X}{L}) \quad (81)$$

At constant hydrogen flux permeating through the membrane (per unit area), expressed in units of current density is given by Fick's first law

$$j_H^0 = FD\frac{C_0}{L} \quad (82)$$

At stop of the charging, hydrogen leaves the membrane, the overall desorption process is represented by Fick's second law

$$\frac{dC}{dt} = D\frac{d^2C}{dX^2} \quad (83)$$

At initial conditions (81) and (82) if hydrogen concentration at entry side drops instantaneously to zero

$$C = 0, X = 0, at\ t > 0$$

on interruption of the charging, the solution to (83) are given in a normalized desorption rate i.e. as a ratio of the desorption rate (j_H) at a given time to the initial steady state permeation rate (j_H^0) as follows:

Exit side (X = L)

$$\frac{j_{H,L}}{j_H^0} = -2\sum_{n=1}^{\infty}(-1)^n \exp\left(-\frac{n^2\pi^2 Dt}{L^2}\right) \quad (84)$$

Or the equivalent

$$\frac{j_{H,L}}{j_H^0} = 1 - \frac{2L}{\sqrt{\pi Dt}}\sum_{n=0}^{\infty}\exp\left(-\frac{(2n+1)^2L^2}{4Dt}\right) \quad (85)$$

Entry side (X = 0)

$$\frac{j_{H,L}}{j_H^0} = 2\sum_{n=1}^{\infty}\exp\left(-\frac{n^2\pi^2 Dt}{L^2}\right) \quad (86)$$

Or the equivalent

$$\frac{j_{H,L}}{j_H^0} = -1 + \frac{L}{\sqrt{\pi Dt}}\left[\sum_{n=1}^{\infty}\exp\left(-\frac{n^2L^2}{Dt}\right) + \sum_{n=1}^{\infty}\exp\left(-\frac{(n+1)^2L^2}{Dt}\right)\right] \quad (87)$$

Where $j_{H,L}$ and $j_{H,0}$ are the desorption rates for the exit and entry side respectively.

Changes in the normalizes desorption rates $\frac{j_{H,L}}{j_H^0}$ and $\frac{j_{H,0}}{j_H^0}$ as a function of the normalized time parameter $\tau = DtL^{-2}$ are shown in figure 18.

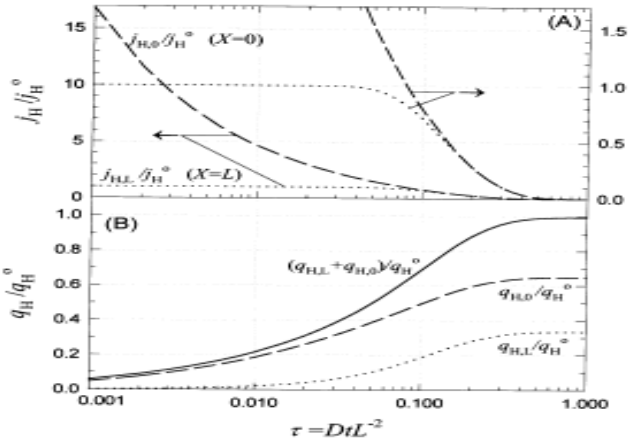

Figure 18: Normalized desorption rates (A) and corresponding amount of hydrogen (B), diffusing out of the exit and entry side of the metal membrane.

To get the amount of hydrogen $q_{H,L}$ and $q_{H,0}$ (in mol H per unit area) leaving the membrane at its exit and entry sides respectively, there is need to integrate (84) and (86) the currents $j_{H,L}$ and $j_{H,0}$, leading to the following:

$$q_{H,L} = \frac{2j_H^0L^2}{\pi^2DF}\left[\sum_{n=1}^{\infty}\frac{(-1)^n}{n^2}\exp\left(-\frac{n^2\pi^2Dt}{L^2}\right) - \sum_{n=1}^{\infty}\frac{(-1)^n}{n^2}\right] \quad (88)$$

And

$$q_{H,0} = \frac{2j_H^0L^2}{\pi^2DF}\left[\sum_{n=1}^{\infty}\frac{1}{n^2} - \sum_{n=1}^{\infty}\frac{1}{n^2}\exp\left(-\frac{n\pi^2Dt}{L^2}\right)\right] \quad (89)$$

At infinity, when $t \to \infty$, the amount of hydrogen desorbed are

$$q_{H,L} = \frac{2j_H^0L^2}{\pi^2DF}\left[-\sum_{n=1}^{\infty}\frac{(-1)^n}{n^2}\right] = \frac{j_H^0L^2}{6DF} \quad (90)$$

$$q_{H,L} = \frac{2j_H^0L^2}{\pi^2DF}\left[\sum_{n=1}^{\infty}\frac{1}{n^2}\right] = \frac{j_H^0L^2}{3DF} \quad (91)$$

Such that the total amount of hydrogen stored in the membrane before the charging interruption is given by

$$q_H^0 = q_{H,L}^{\infty} + q_{H,0}^{\infty} = \frac{j_H^0 L^2}{2DF} \quad (92)$$

A membrane with both diffusible and trapped hydrogen:

In order to minimize surface processes, if a partial build-up or desorption transient is used and if the hydrogen concentration at the input side settles immediately at a new value after the change of cathodic current, the equation to calculate hydrogen diffusivity can be given by

Decay:

$$\frac{j_P - j_{P2}^{\infty}}{j_{P1}^{\infty} - j_{P2}^{\infty}} = 1 - \frac{2L}{\sqrt{\pi Dt}} \sum_{n=0}^{\infty} \exp\left(-\frac{(2n+1)^2 L^2}{4Dt}\right) \quad (93)$$

Build-up:

$$\frac{j_P - j_{P1}^{\infty}}{j_{P2}^{\infty} - j_{P1}^{\infty}} = \frac{2L}{\sqrt{\pi Dt}} \sum_{n=0}^{\infty} \exp\left(-\frac{(2n+1)^2 L^2}{4Dt}\right) \quad (94)$$

Where j_{P1}^{∞} and j_{P2}^{∞} are the initial (t = 0) and final steady state permeation rate ($t \to \infty$) and j_P is the permeation rate at a chosen time $t > 0$.

3.6.2 Nanis and Namboodhiri [1]

They developed the mathematical model for desorption of hydrogen from a permeation test according to Devananthan and stachursky method. At steady state condition, without the presence of traps, a triangular distribution is assumed as initial condition for desorption.

$$C = C_0\left(1 - \frac{x}{L}\right)$$

The solution to Fick's second law is obtained following two extreme cases:

1) The **slowest possible extraction** is based on the assumption that the input side became completely impermeable to hydrogen after cathodic current interruption and hydrogen can be extracted only from the anodic side (exit side)

2) In the **fastest possible extraction** the concentration at the cathodic side (input side) is considered to drop instantaneously to zero upon input current interruption and hydrogen can escape from both the input and the exit sides.

Slow decay:

Boundary conditions: $\frac{dC}{dX} = (0, X) = 0, \ \ at\ (t > 0) \quad and \quad C = 0, X = L, \ \ at\ (t \geq 0)$

The flux at the exit side is given as:

$$\frac{j_t}{j_\infty} = 1 - 2\sum_{n=0}^{\infty}(-1)^n erfC\frac{(2n+1)L}{2(Dt)^{0.5}} \tag{95}$$

Fast decay:

The flux is given as:

$$\frac{j_t}{j_\infty} = 1 - 2\sum_{n=0}^{\infty}\frac{1}{\sqrt{\pi}}\frac{L}{\sqrt{Dt}}e^{-\frac{[2n+1]^2L^2}{4Dt}} \tag{96}$$

Separate equations for the two fluxes (anodic and cathodic sides) in a fast decay model:

i) Input side:

$$F_{IN} = -D(\frac{dC}{dX})_{X=0} \quad = -\frac{2DC_0}{L}\{\sum_{n=1}^{\infty}\exp(-\frac{n^2\pi^2Dt}{L^2})\} \tag{97}$$

ii) Exit side:

$$F_{EX} = -D(\frac{dC}{dX})_{X=L} \quad = -\frac{2DC_0}{L}\{\sum_{n=1}^{\infty}(-1)^n\exp(-\frac{n^2\pi^2Dt}{L^2})\} \tag{98}$$

The total quantity per unit area of hydrogen diffusing out from each surface Q_E is obtained by integrating the flux over the entire range of time.

$$(Q_E)_{X=0} = \frac{C_0L}{3} \qquad (Q_E)_{X=L} = \frac{C_0L}{6} \qquad and \quad Q_{TOT} = \frac{C_0L}{2}$$

Chapter 4: Experimental.

4.1 Introduction

In the previous phase of this research, hydrogen permeation test based on Devanathan Stachurski method were carried out on X65 and F22 steel samples at 20°C [6].

Apparent diffusion coefficient of hydrogen was measured in the range of 2 X 10^{-11} m^2 s^{-1} and desorption technique was adopted in order to understand the exiting profile of hydrogen from the sample. Permeation behavior of same specimens at 20 ± 2°C showed that the time to breakthrough for both first and second permeation transient was almost the same [6, 39].

In the current work, all experimental permeation tests were carried out at 40 ± 2°C, with all other condition and specimens same as in the previous phase.

4.2 Materials

The samples used for this phase of the research were carefully extracted with the aim of simulating the diffusion of hydrogen in the flow direction that develops in a commercial produced seamless pipe in operation, as shown in figure 19.

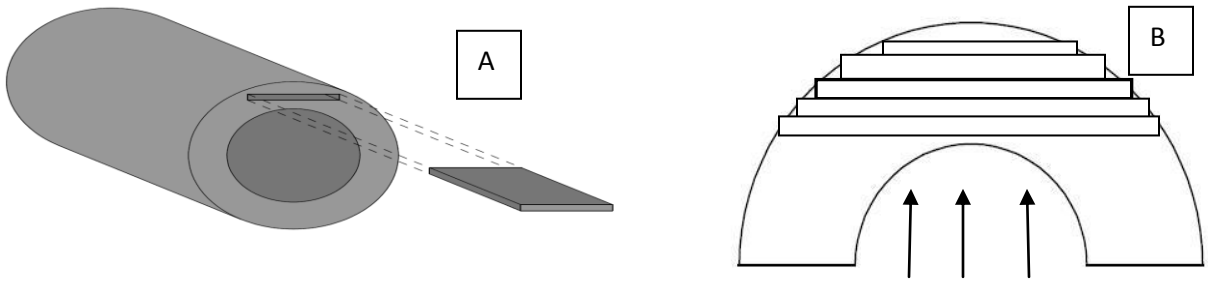

Figure 19: A) Direction of extraction of sample from a seamless pipeline [39]. B) Direction of flow of hydrogen atoms, which is radial to the cut samples from the seamless pipeline.

The materials used for this research are namely:

- Micro- alloyed C-Mn steel, API 5L X65,

- Low alloyed 2 ¼ Cr-1 Mo steel, ASTM A 182 F22,

X65 pipeline steel with the chemical composition shown in table 4. The metallurgical observation shown in figure 21, indicate that the microstructure of the steel contains ferrite and carbides, with the latter randomly distributed in the bulk material. The inclusion characteristics for both orientations i.e. longitudinal and transverse, showed that [40]

- Inclusion shape is round as expected for sour gas material, since it was treated with calcium, thereby spheroidizing all inclusions shown in figure 20.
- Longitudinal and transverse orientations do not show any difference either in density or in diameter.
- There was no central segregation present.
- The inclusion density was high.

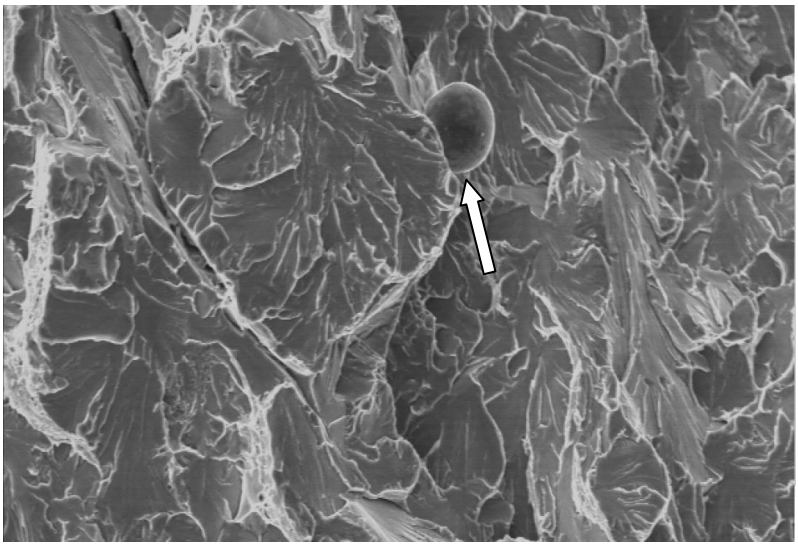

Figure 20: showing the nature (round) of the inclusions in API 5L X65 steel.

F22 pipeline steel with chemical composition also shown in table 4, has a microstructure that is typical of tempered lath martensite, with elongated ferrite grains and finely dispersed carbides. Inclusion characteristics showed the same properties as listed above for API 5L X65 steel. The composition of the steels is given as follows in table 4:

Table 4: The composition of X65 and F22 pipeline steels

Steel	Element%											
	C	Si	Mn	S	P	Cr	Mo	Ni	Nb	V	Ti	Al
X65	0.11	0.28	1.18	0.007	0.017	0.17	0.15	0.42	0.023	0.06	<0.01	0.03
F22	0.14	0.11	0.43	0.001	0.003	2.25	1.04	0.08	0.023	<0.01	<0.01	0.04

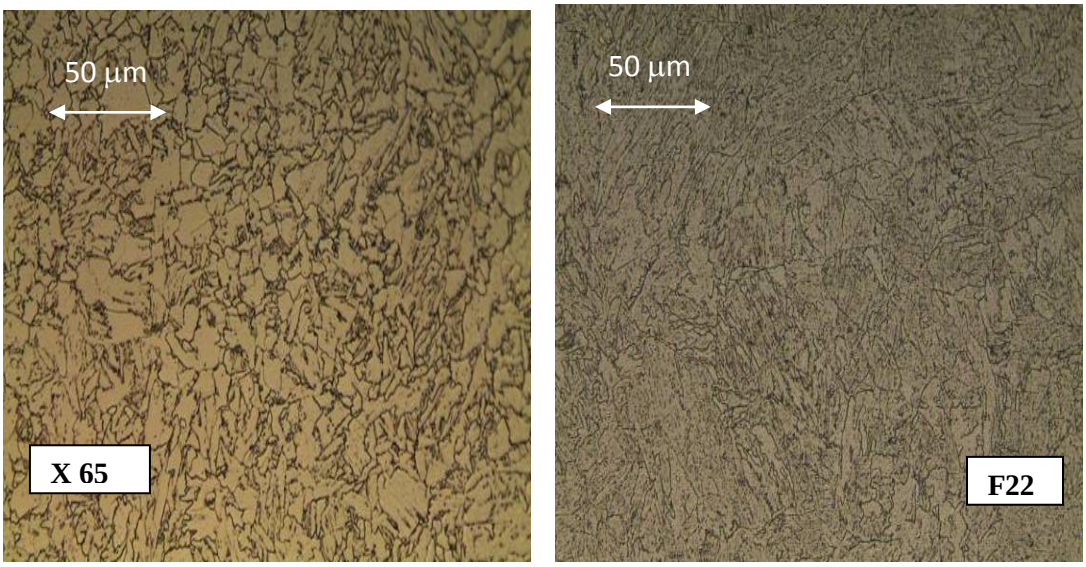

Figure 21: OM microstructures of both X65 and F22.

The mechanical properties of the as received pipeline steel are given in table 5:

Table 5: The mechanical properties of X65 and F22 steels.

Material	σ_{ys} (MPa)	σ_{ts} (MPa)	E (GPa)	A (%)
F22	468	592	206.5	20
X65	511	609	206.2	21

Specimen surface preparation: The samples used were obtained as shown in figure 18. Sizes varying from 200 mm to 300 mm and thickness varying from 1 mm to 2 mm were cut from the base material. The specimens were subjected to heat treatment at a temperature of 350^{o}C for 3 hours to remove any possible residual hydrogen. On cooling the specimens were manually polished with SiC emery paper up to grade 1200 and clean with distilled water and alcohol. The material preparation conditions of the specimens were selected to reproduce the real use conditions in industrial applications where the material is not annealed. Copper wire was soldered on the tip of the specimen for connection.

4.3 Permeation test

Permeation tests were carried out on a modified twin compartment Devanathan cell, according to ISO 17081, constructed with glass and polycarbonate material as junction cups between two compartments which hold the samples with separated O-ring for sealing. The ratio of exposed area on the oxidation side was taken to 90% roughly which corresponds to ratio of radius to thickness 5:1 as was recommended by this standard as well; the composition of the charging solution and conditions that was used for our test was simulated as written below.

Cathodic charging solution:

- 0.2 mol L^{-1} of CH_3COONa (32.8 g L^{-1}) + 0.4 mol L^{-1} of CH_3COOH(12.0 g L^{-1} =11.6 mL L^{-1}), buffered at pH 4.2.
- Complete de-aeration of cathodic solution was achieved by purging with pure nitrogen gas N_2.
- Temperature T = 40 $\pm$ 2 ˚C
- Electrochemical condition: Galvanostatic charging: 0.5 $mAcm^{-2}$

Anodic Solution:

- 0.2 mol L^{-1} sodium hydroxide (NaOH)
- pH $\geq$ 13
- Temperature: T = 40 $\pm$ 2 ˚C

Pre-passivation; before the commencement of diffusion test by

- Immersion: submerged in 0.2 mol L^{-1} NaOH for 1h at T = 65 $\pm$ 2 ˚C
- Anodic polarization: carried out in 0.2 mol L^{-1} NaOH till the attainment of a low current (0.1 $\mu A/cm^2$) with +180 mV vs Ag/AgCl within the anodic compartment.
- Electrochemical condition; Potentiostatic: +180 mV vs Ag/AgCl

Pre-passivation steps were carried out to reduce the background current to the minimum prior to charging of the specimen. This is achieved by a decrease in the amount of current passing through the created passive film with time. Low back ground current eliminates superficial impedance to hydrogen flow and makes constant the boundary conditions, which in the traditional permeation is achieved by coating of the exit side with palladium. The procedures, duration and the operating temperatures used during pre-passivation were established after several tests, in the previous phase of this research [39].

The prepared specimens (Working electrode, W) were used as membrane for the hydrogen permeation measurements using the electrochemical permeation technique. The specimen is initially pre-passivated by immersion, after an hour it is mounted between the two compartments of the cell and anodically passivated over the exposed area as determined by the O-ring. At the attainment of the lowest passivity current, the cathodic (charging/entry) compartment was connected. The cathodic solution was introduced into the cathodic compartment. The entry side of the specimen was continuously polarized by the galvanostat in the cathodic solution at a constant charging current of $0.5\ mAcm^{-2}$. The electrochemical reactions occurring on the surface of the specimen during cathodic polarization correspond to the hydrogen evolution reaction as mentioned in section 3.2.

A fraction of the hydrogen is absorbed and diffuses through the specimen and the flux of hydrogen diffusing through the specimen was continuously monitored on the anodic compartment. On the exit side the specimen was potentiostatically maintained at a constant potential of +180 mV vs Ag/AgCl in the anodic solution. Applying this constant potential was to ensure that all hydrogen atoms emerging on the exit side is ionized and that the oxidation current was diffusion controlled, such that the measured anodic current density was that of hydrogen permeation (flow) rate. Cathodic charging current density was applied under galvanostatic charging until a steady current condition was attained in the cathodic compartment. During this period of hydrogen charging (20 hours), the cathodic potentials at the cathodic compartment and the hydrogen oxidation (passivity) current at the anodic compartment were measured.

On imposing of cathodic current at the cathodic compartment, after a short time (time to break through) there was observed a rise in the permeation transient, which increased until reaching a maximum value, then it gradually decrease to a steady state in approximately 10 h at this

temperature, but the permeation test was allowed for 20 h in order to be sure that all possible trap sites has been fully saturated before the second charging. All the permeation transients obtained in this research showed a maximum; this value was used to calculate D_{app}. It is worthy to note that the occurrence of a maximum in the build-up permeation transient was observed earlier at the first part of the research (H permeation study at 20^{o}C) [39].

On attainment of a steady state of the anodic current, the cathodic current was interrupted and a decay transient was followed. Again on attainment of steady state of anodic current a second charging with the same current density and permeation condition was followed. This was done in order to compare the hydrogen permeation behavior with the traps fully saturated and the presence of irreversible traps, if present.

Several tests were carried out with specimens of varying thickness at the specified temperature, with a constant environmental condition. The conditions of the tests together with most of the results are reported in the appendix.

4.3.1 Experimental cell

The permeation cell is composed of an electrolytic cell with two compartments. This two double wall glass compartments of the cell are separated by two clamps made of methyl polymetacrylate (Perspex) having flanges and rubber O-rings which determines the exposed area of the specimens to the electrolyte on each side. The exposed diameter to the electrolyte on the entry side of the membrane is 1.24 mm for 1 mm and 3.2 mm for 2 mm thick specimens respectively. Both compartments were equipped with a platinum coil wire as a counter (C) electrode. On the entry side (cathodic), the counter electrode is connected to the galvanostat, which supplies the charging current, while on the exit side (anodic) it is connected through a 10.1 KΩ "shunt" resistor to the potentiostat, which regulate the potential for passivation and measurement of hydrogen flux, as shown in figure 22.

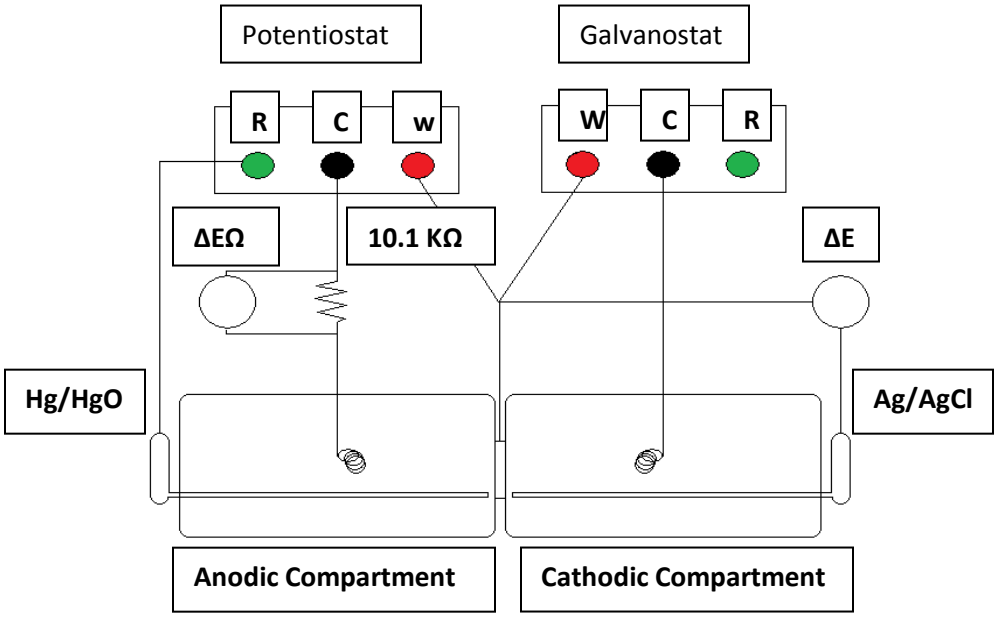

Figure 22: Permeation cell.

A mercury/mercury oxide (Hg/HgO) electrode was introduced to the anodic compartment and a silver/silver chloride (Ag/AgCl) electrode to the cathodic compartment, both serving as a reference (R) electrode. The cathodic (charging/entry) compartment was connected to a floating ground galvanostatic PGP201 while the anodic (exiting) compartment was connected to a potentiostat AMEL Mod. 1480/A. These two were connected to a computer soft-ware which was used for data collection and analysis. The computer soft-ware was used to measure the anodic current, the cathodic potentials and cathodic discharge current, in some occasions, per the required duration. In our case, 30 seconds between two following measurements was mostly used. Nitrogen gas was continuously bubbled into the cathodic solution in a tank and then passing through the cathodic solution in a reservoir for de-aerating the solution before and during the test. De-aerated water is circulated from a cryothermostat Julabo F33, through the double jacket and back in order to maintain a constant temperature of ($T = 40 \pm 2°c$) in both compartments of the cell, as shown in figure 23.

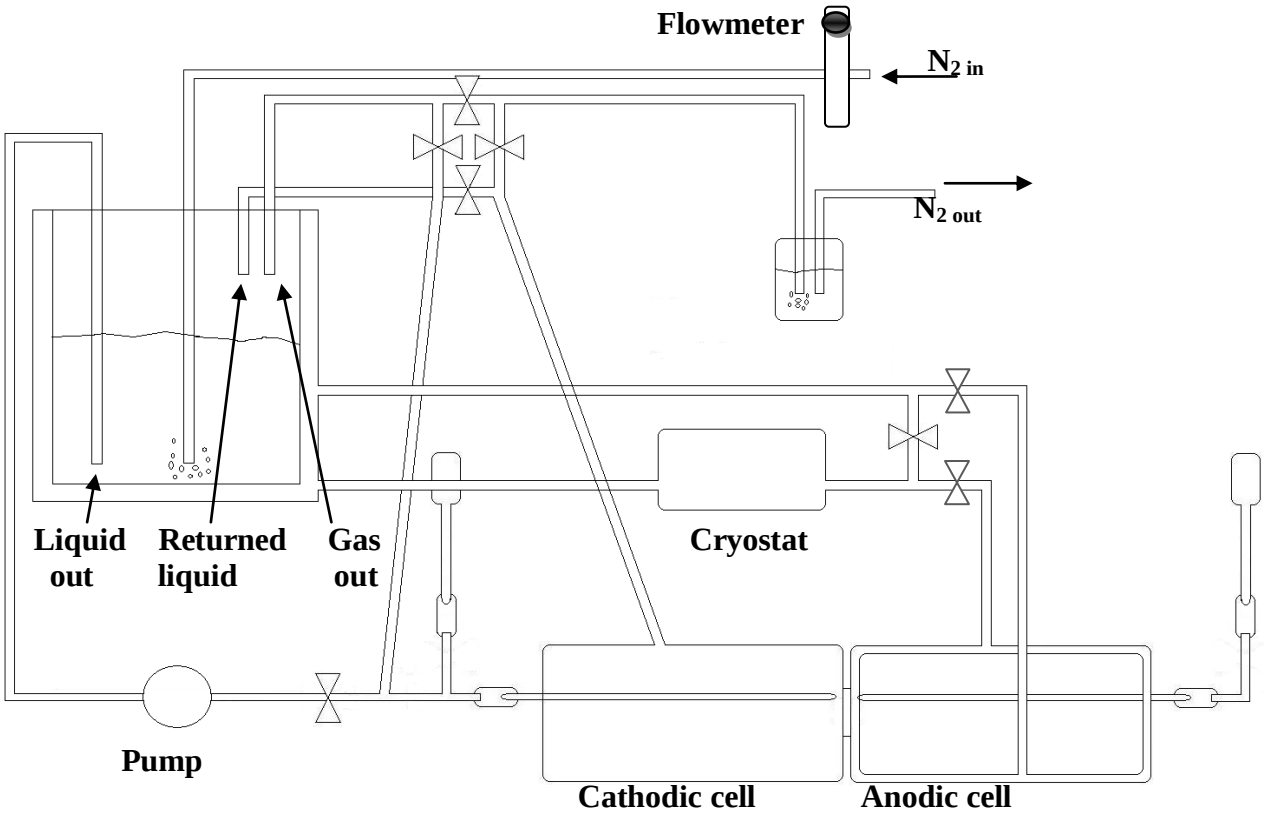

Figure 23: Process flow diagram of the permeation test.

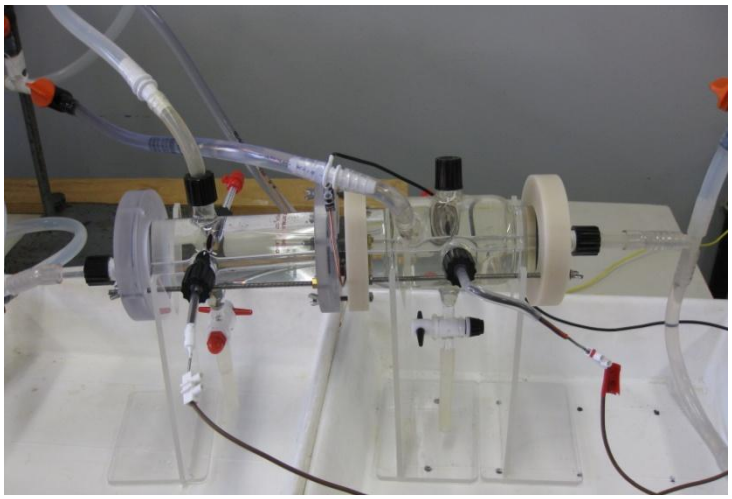

Figure 24: A picture of the permeation cell used in this experiment.

4.3.2 Partial build-up/desorption transient

According to Zakroczymski [28] the only factor that control permeation rate should be diffusion, but due to the extremely high diffusivity of hydrogen in iron, it is difficult to avoid this undesirable effect of slower surface processes, with respect to hydrogen entry, and trapping, which involves hydrogen transport. These surface effects can be eliminated by applying long uninterrupted cathodic polarization, while the trapping effects can be minimized by successive partial build-up transient of cathodic polarization. To this effect we carried out partial build up and desorption analysis in order to stimulate the behavior of lattice diffusion of hydrogen. This was carried out as follows

- **With intermediate discharge:**

  As the permeation transient attains a steady state, while charging with 0.5 mA cm^{-2}, the charging current is increased to 1.0 mA cm^{-2}. On arriving to the new steady state, the charging current is reduced to 0.1 mA cm^{-2}

- **Without intermediate discharge:**

  As the permeation transient attains a steady state, while charging with 0.5 mA cm^{-2}, the charging current is increased to 1.0 m Acm^{-2}.

Potentiostatic test was carried out to confirm the partial build-up and desorption transient to have an idea about the lattice diffusion. It was observed that after maximum hydrogen permeation current at -700 mV Vs Ag/AgCl was reached, the potential was decreased without intermediate hydrogen discharge. This shows that if the electrochemical conditions of the cathode are changed when a steady state condition of hydrogen diffusion has been reached, there is almost an immediate variation of anodic current. So if there is a small increase in the hydrogen generation current, it leads to a rapid increase in hydrogen permeation current and a new steady state is reached in a very short time. This effect is a variation from Fick's law, so a partial build up diffusion modeling is required.

To this effect a partial permeation build-up transient for pre-charged F22 specimen was performed under the potentiostatic charging from -700 mV to -750mV and another test was perform with F22 specimen under galvanostatic charging from 0.5 to 1 mA cm^{-2} same with section 4.2.3 (2). This test was repeated for X65 specimen.

4.3.3 Desorption

As the anodic current attains a steady state during first charging transient, the cathodic current is interrupted. The decreasing anodic current density was continually measured throughout the desorption test. In most of the desorption test, the anodic current density was measured from the anodic compartment only. In this case the cathodic compartment is dismantled and the exposed surface of the specimen washed with distilled water and dried with N_2. But in other times, there was an attempt to measure the hydrogen discharge current from both compartments. The procedure remains the same at the anodic compartment, while at the cathodic compartment, the cathodic solution was extracted and replaced with anodic solution in a process that lasted approximately 5 minutes for all test. At completion, cathodic discharge current measurement commence at the cathodic compartment with same anodic potential that was applied on the anodic side (+180 mV vs. Ag/AgCl), as the hydrogen atoms are diffused out from both anodic and cathodic sides of the specimen at the same time. The anodic current density measured during these periods of discharging show the desorption transients. More research is required in this area of measurement of hydrogen discharged current from cathodic compartment experimentally in order to prevent the time lost during the change over, to obtain a good analysis.

Chapter 5. Results and Discussions

5.1 Hydrogen Diffusivity.

For all specimens, permeation transients showed the sigmodal shape as shown in figure 25. Furthermore most of the experimental results obtained in this thesis work are recorded under the appendix section. To analyze the hydrogen permeation current data, from the mathematical equations mentioned in section 3.6, calculations of such parameters as hydrogen diffusivity and sub-surface hydrogen concentration was made.

On application of cathodic current, after a certain time (time to break through) a rapid increase of anodic current was observed. Most of build-up transients obtained in this research showed a maximum value between 4 to12 µA cm^{-2}.

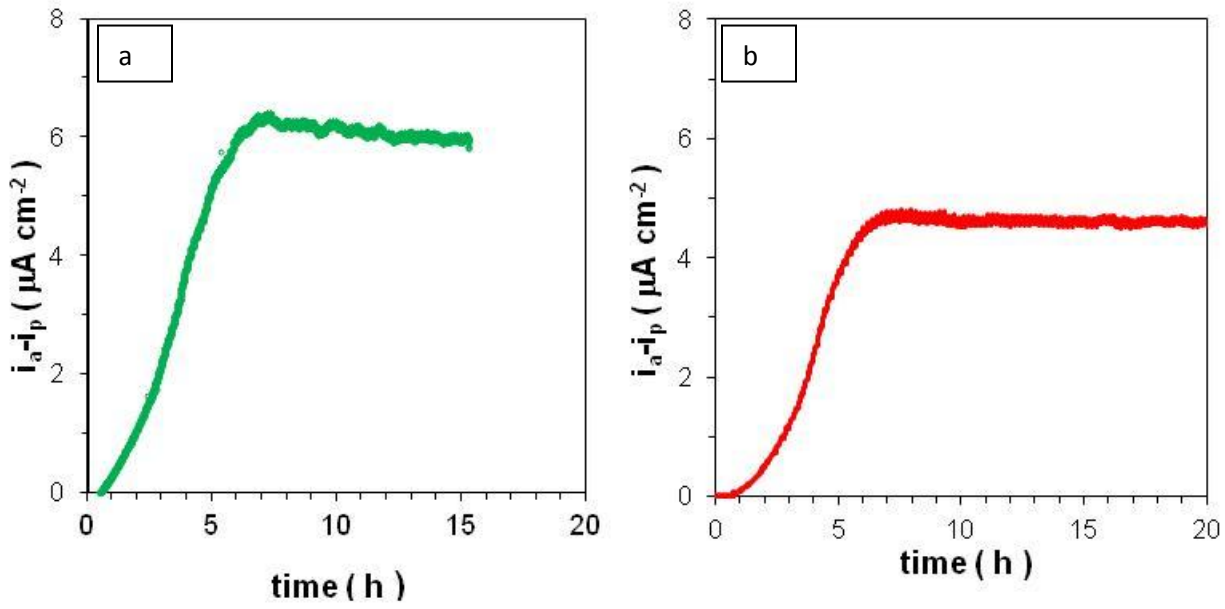

Figure 25: First hydrogen permeation build-up transients for a) F22 1.25 mm and b) X65 1.25 mm samples

If D_L (lattice diffusion as described earlier) varies from the beginning of the test such that D(t) is decreasing along the permeation curve by the passing of time, in such case the diffusion coefficient calculated is considered as apparent (effective) diffusion due to the possible effects of surface processes and trapping. D_{app} is calculated using any of the methods listed in section 3.4.4 above. In particular using breakthrough time to calculate D_{app} as in figure 26, has shown a

decreasing trend with increasing of time, as in table 6. Applying the mathematical relation derived from Fick's solutions for the boundary conditions given as

$$D_{app} = \frac{L^2}{M \times t}, \qquad (99)$$

Where M is a constant depending on the time value t, chosen in the diffusion transient as stated in table 6. D_{app} is calculated using any of the ratio between the current density and the steady state current density j/j_∞, which imposes a corresponding value of time e.g. for 1% the ratio, M is 25. In this research all calculations of D_{app} was done with 1%, 10%, 63% and tangent values of M.

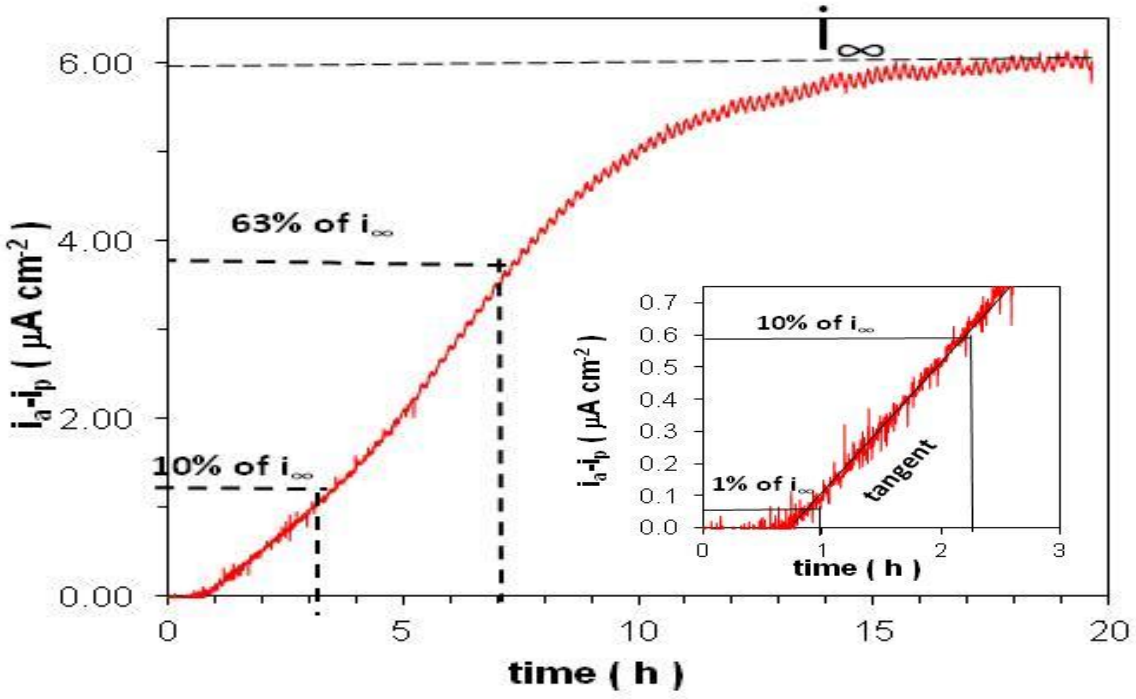

Figure 26: showing the % permeation rate for the first transient of F22.

Table 6: showing the relationship between j / j_{∞} τ and M.

$\frac{j}{j_{\infty}}$	1%	10%	30%	40%	63%	80%	90%
$\tau = \frac{D \times t}{L^2}$	0.04	0.06	0.10	0.12	0.17	0.23	0.30
$M = \frac{1}{\tau}$	25	15.30	10	8.33	5.98	4.37	3.33

In order to follow permeation test with traps fully saturated, at steady state condition cathodic current was interrupted and charging solution evacuated. On reaching the same passivity current value of first stage, 2nd build-up transient was applied using the same cathodic current density that was used previously. Since irreversible traps (saturable sites) are filled during the 1st build-up transient, quicker permeation in a case of time to break through was observed, which could be attributed to the presence of irreversible traps.

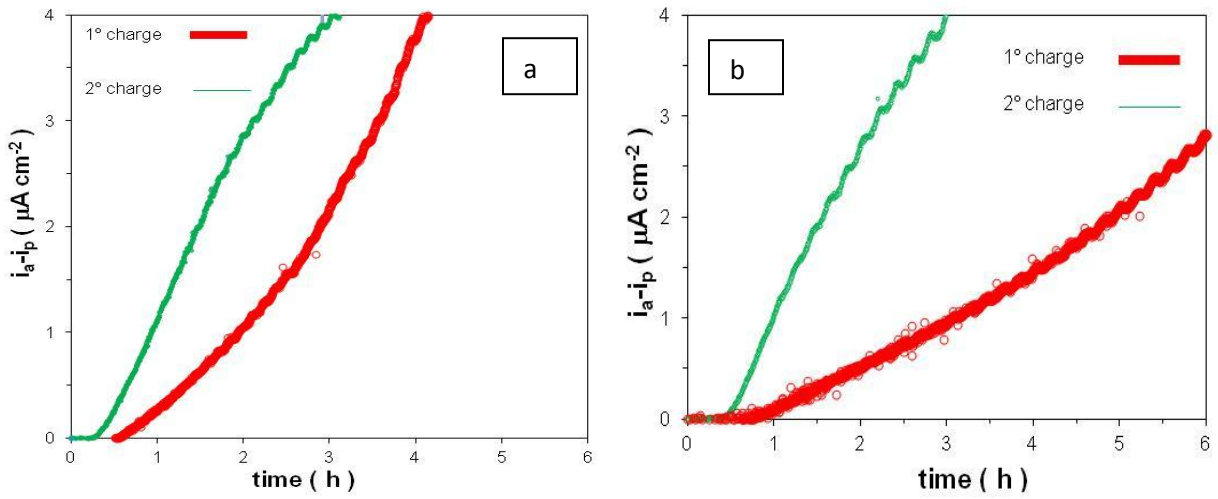

Figure 27: Time to break-through for 1st and 2nd build-up transients at 40°C: Curve a) F22 (1 mm) and curve b) X65 (1 mm)

As it can be seen in figure 27, the first rise of the curve considered, that corresponds to arrival of hydrogen to the outer surface, represents a delay time t_b, in which in our experimental conditions

by considering 1% $j\infty$ criteria this time is in the range of 1900 seconds for 1st transient and 1000 seconds for the 2nd transient. Thus the second transient time to break through was shorter than that of the first at this temperature. This may explain the activation of trapping during the permeation, i.e.; fast and then slow process.

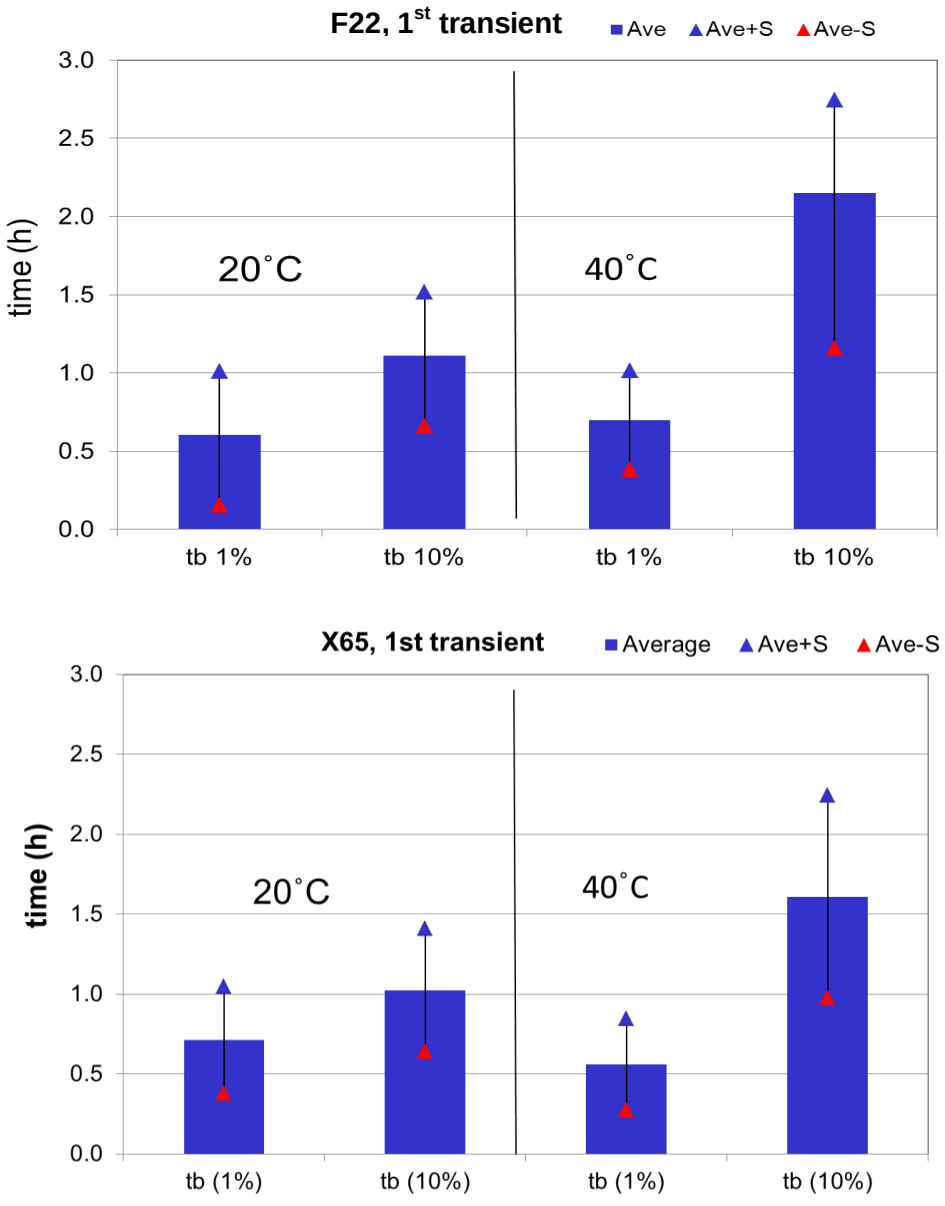

Figure 28: Comparison of time to break-through for F22 and X65 (1st transient) at 40 and 20°C

According to literature, permeation transients could be given in normalized shape. For this purpose permeation flux was plotted against non-dimensional form of time, τ which is given

by $D \times t / L^2$ [5]. Normalized shape of permeation transients for both X65 and F22 steel samples are shown in figure 29. Most of the build-up permeation transients reached the maximum value instead of monotonic trend. This could be justified by difficulties to maintain constant electrochemical conditions on the entry side of the sample during prolonged hydrogen charging.

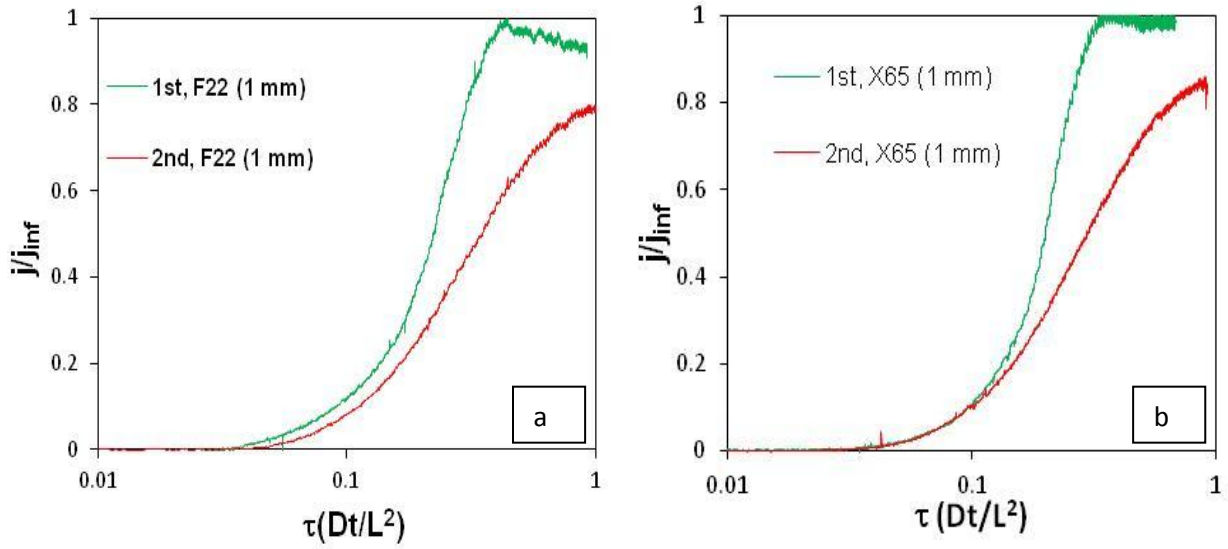

Figure 29: Normalized hydrogen permeation transients computed for both 1st and 2nd transients. Curve a) F22 and curve b) X65

Note that the maximum permeation current density was used for diffusivity calculation based on the various methods mentioned before. Comparing the corresponding time to break through of the first and second permeation transient indicates the presence of irreversible traps if the second transient time is shorter or faster.

All permeation transients showed independence of thickness effect, which is a guarantee that hydrogen transport is controlled by diffusion.

The results obtained by calculating D_{app} for all the specimens are in the range of 1 to 4 $\times 10^{-11}$ m^2s^{-1} for X65 and F22. These results are tabulated in the histogram shown in figure 30. It is observed that in both cases a) F22 and b) X65, the highest D_{app} value was obtained at the beginning of the test (tangent) and decreases through 1% to 63%. It seems there is a trend in which diffusion coefficient decreases for both 1st and 2nd transients that could be attributed to the trapping effect. If traps at the beginning of the test are not filled, diffusion will take place quickly

and then trapping process will overcome the diffusion of hydrogen thereby slowing it down. This may strongly depends on the time to equilibrium between the lattice sites and reversible traps. In other word, if equilibrium between lattice site and reversible traps happens very fast trapping effect will control the transport of hydrogen inside the metal.

Table 7: showing the calculated D_{app} for F22 and X65.

		tg	**1%**	**10%**	**63%**
Material (1 & 2 mm)	**At 40°C**	$D_b \pm St.dev$ $10^{-11}(m^2 s^{-1})$	$D_b \pm St.dev$ $10^{-11}(m^2 s^{-1})$	$D_b \pm St.dev$ $10^{-11}(m^2 s^{-1})$	$D_{lag} \pm St.dev$ $10^{-11}(m^2 s^{-1})$
F22	1st	2.31 ± 0.55	2.14 ± 0.69	1.34 ± 0.72	1.18 ± 0.40
	2nd	5.31 ± 2.18	3.69 ± 1.31	3.21 ± 1.45	2.01 ± 0.98
X65	1st	3.47 ± 1.19	2.87 ± 1.13	1.34 ± 0.49	1.24 ± 0.54
	2nd	3.28 ± 1.30	2.67 ± 0.92	2.24 ± 1.48	1.86 ± 1.29

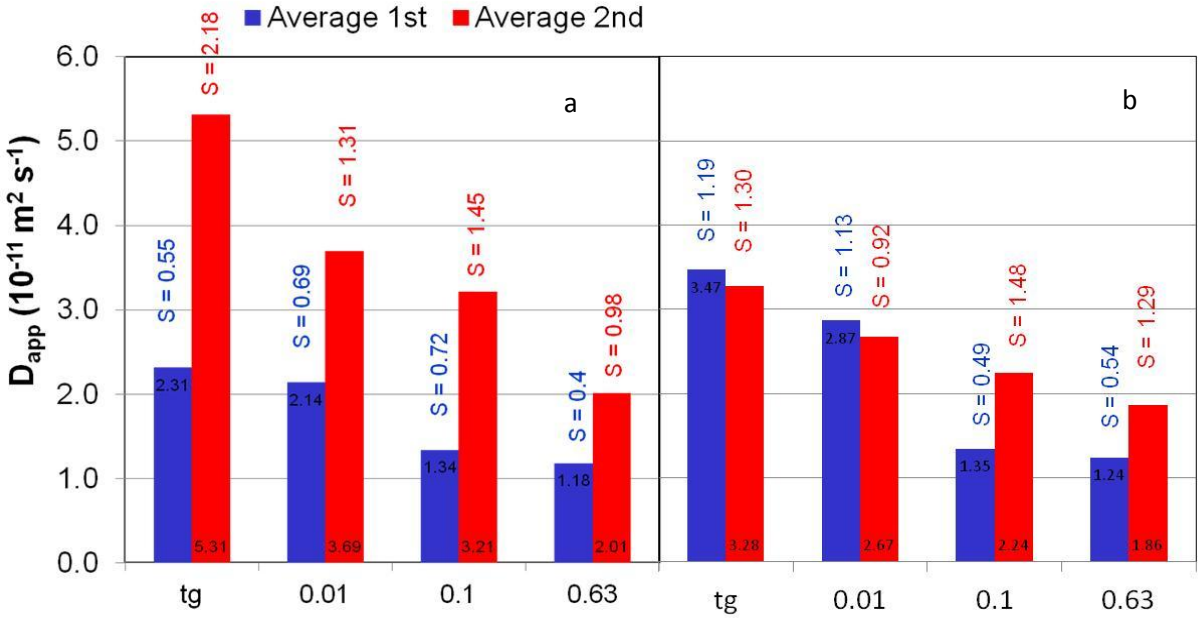

Figure 30: Histogram showing the variations in D_{app} with percentage of dimensionless flux for both F22 (a) and X65 (b).

Comparing the values obtained for time to break through at 40°C with data obtained before at 20°C have not shown changes in the case of t_b for 1st transient and it is also observed at 40°C, that the 2nd permeation build-up is quicker than that of 20°C. Moreover by passing of time, 10% j_∞, corresponding time value increases significantly at 40°C compared to the value obtained at 20°C both for F22 and X65 as can be seen in figure 28.

Comparing the results of D_{app} obtained at 40°C with those obtained at 20°C, as shown in figure 31, it was observed that the trend of decreasing D_{app} from tg through to 63% was maintained and it was observed also that the results obtained at 40°C were in the same range of those obtained at 20°C for both F22 and X65 materials. This can be justified by the fact that the expected ratio between the diffusion coefficient at 20°C and 40°C, on the basis of the activation energy (15.5 KJ/mol) is 1.5, that is in the same order of magnitude of the scattering of the results.

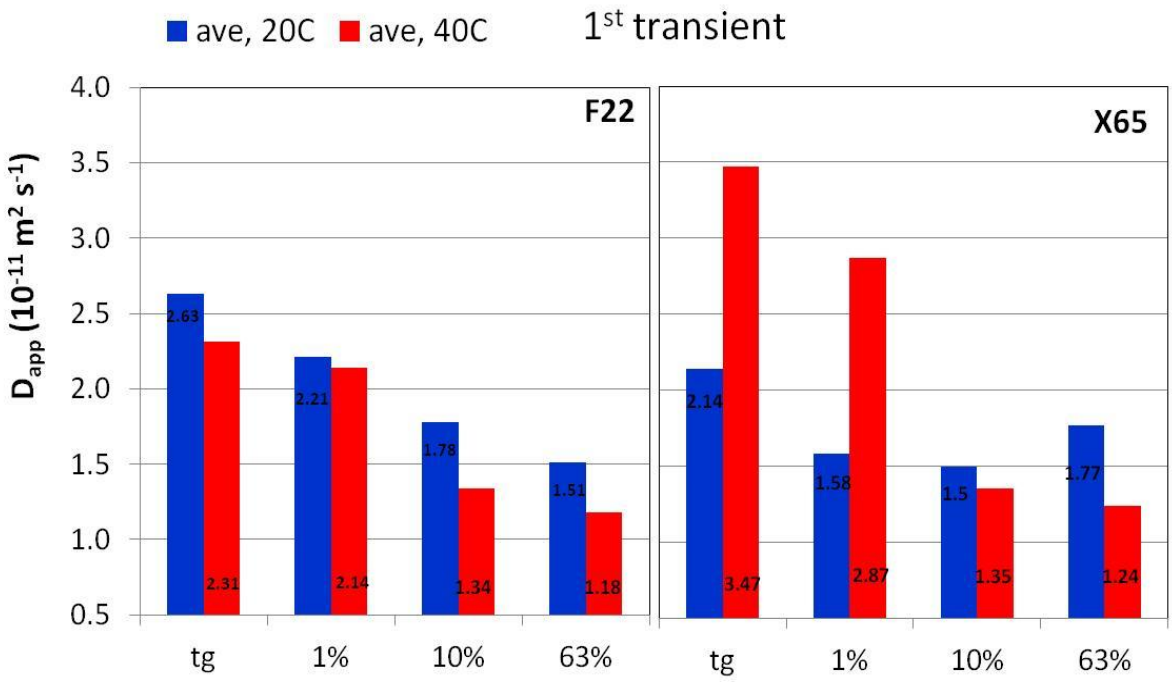

Figure 31: Histogram comparing the results of D_{app} obtained at 20°C with those obtained at 40°C for both F22 and X65.

5.2 Hydrogen Concentration

According to literature [10], the sub-surface hydrogen concentration C_o is established instantaneously. During the permeation test hydrogen subsurface concentration is supposed to be constant, but what is observed is, on imposition of cathodic current density under galvanostatic charging, concentration reaches a constant value during prolonged charging. The sub-surface hydrogen concentration C_o, very close to the cathodic side can be calculated with known apparent hydrogen diffusion coefficient, D_{app} with the equation given as follows.

$$C_o = \frac{i_\infty L}{nFD_{app}} \tag{100}$$

Where i_∞ is the steady state permeation current density, n is the number of electrons transferred, F is the faraday's constant and L (m) is the thickness of the specimen.

Comparing the results of C_0 with those obtained at 20˚C, show an increasing trend with increasing temperature for both steel materials as seen in figure 32. It might be attributed to the higher steady state permeation current density at 40˚C and variation of apparent diffusivity from the beginning (1% i_∞) to end (63% i_∞) along the permeation build-up transient but tends to a constant value at prolonged charging as can be seen from the difference between (10% i_∞) and (63% i_∞) criteria of D_{app} at 40°C in figure 30.

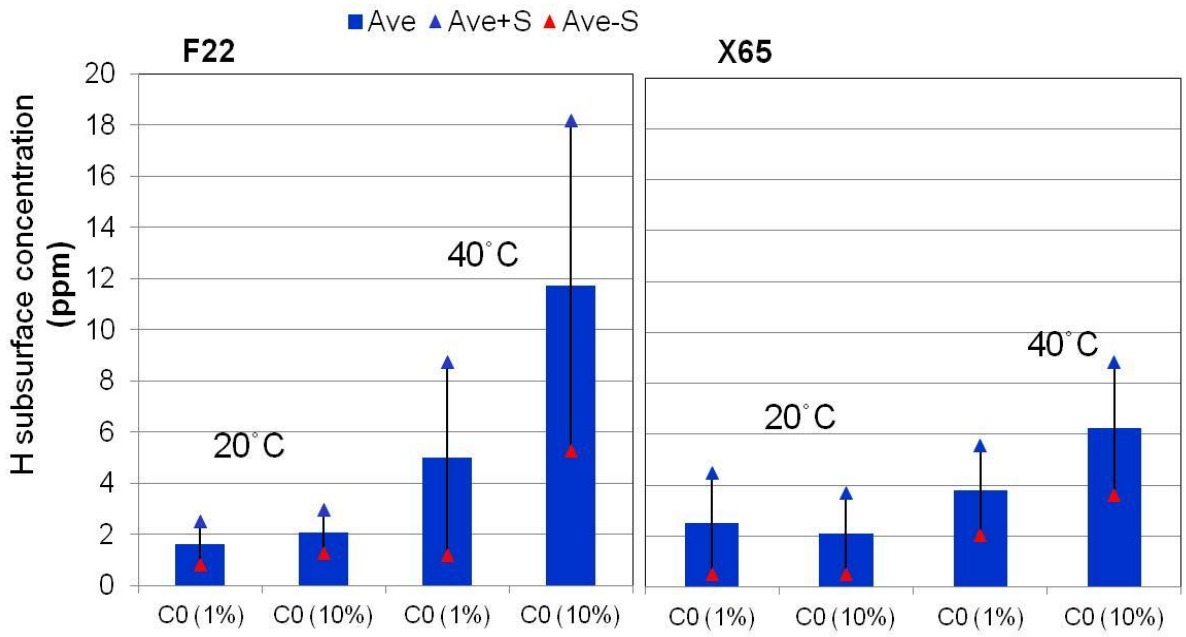

Figure 32: Histogram comparing the results of C_o for F22 and X65 at temperatures of 20°C and 40°C.

5.3 Electrochemical behavior

During galvanostatic polarization at 40°C, cathodic potential variations were observed. The potential drifted towards more negative values with increasing time (from -600 to -850 mV Vs Ag/AgCl) as shown in figure 33, this was the same that was observed at 20°C. Since temperature, pH and de-aeration were well controlled testing parameters, this scattering can be attributed to surface effects. In general there was the observation of initial small hydrogen permeation at start followed by a fast growth with a simultaneous drop in potential. The results obtained here were the same when potentiostatic polarization was carried out. In addition, cathodic polarization curves shows -240 mV/decade of Tafel slope which is much higher than all hydrogen evolution mechanism which consider hydrogen coverage as low (-120 mV/decade). Cathodic polarization curve obtained during hydrogen permeation test, in which for each test, as received samples (hydrogen free membrane) was used is given in figure 34.

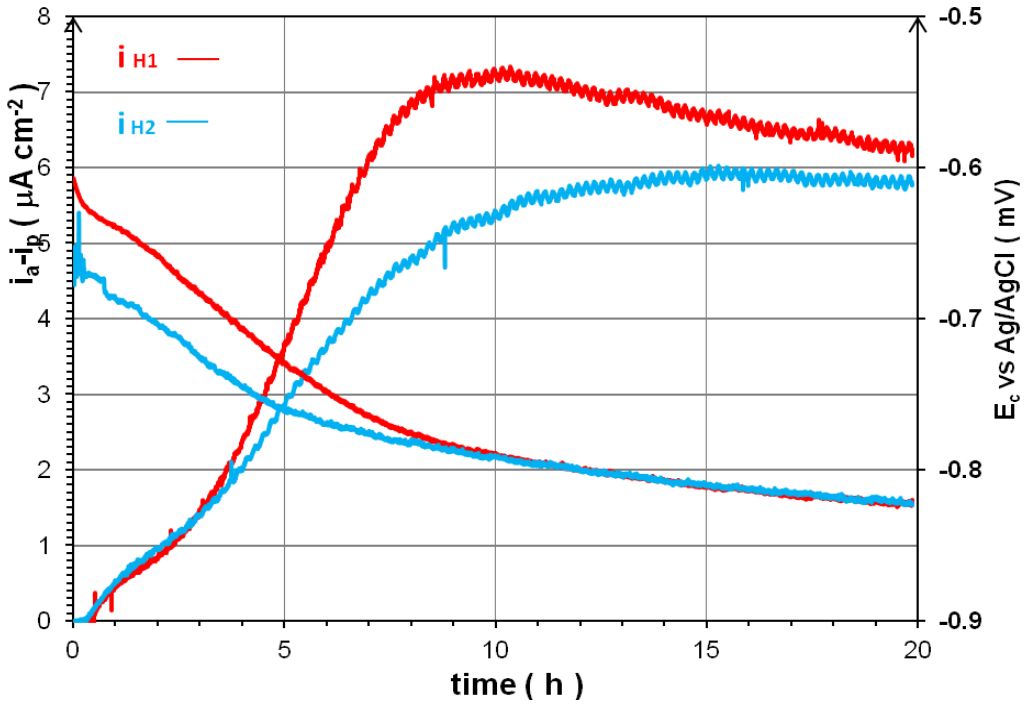

Figure 33: variation in cathodic potentials (E_c), moving towards a more negative value with time for both 1st and 2nd charging with 0.5 mA cm^{-2}.

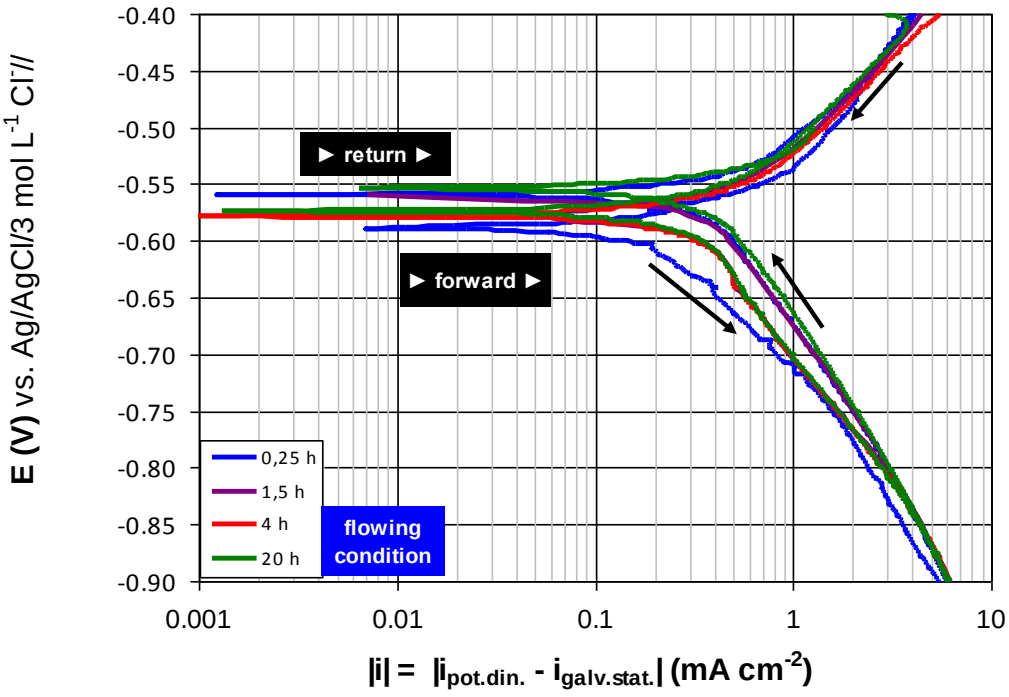

Figure 34: Electrochemical behavior of F22 steel cathodically polarized at 0.5 mA cm^{-2} after 0.25-20 hours, in flowing (10 L h^{-1}) acetic solution at 40°C (cyclic potentiodynamic test, scan rate: 1 mV s^{-1})

5.4 Trapped Hydrogen

Irreversible trapping. As it was mentioned previously, in some cases it was found that the 2nd permeation transient was faster than the 1st one, indicating a possible effect of the irreversible trapping. This effect was not always reproducible and was found only in some cases at 40°C (Figure 27); this effect was not recorded in the tests carried out at 20°C in previous phases of the research. The effect of irreversible trapping is not expected in these type of steels, since they are 'sour grade' material in which the inclusions are shaped round with rare earth metals and density of traps are very low

Reversible trapping. A complete decay is sensitive to hydrogen release from reversible traps. In other word experimental hydrogen desorption transient represents total amount of hydrogen from reversible traps and interstitial lattice sites. Since theoretical desorption transient is a representative of hydrogen releasing from lattice sites, comparison of experimental and theoretical hydrogen desorption curve can give the hydrogen balance inside the specimen (hydrogen in lattice sites and hydrogen in reversible traps). In some tests the cathodic current was increased from 0.5 to 1 mA cm^{-2} after that maximum hydrogen permeation current was reached. The main result is that if the electrochemical conditions on the entry side of the membrane are changed, after that steady state condition has been reached, the variation of anodic current starts almost immediately. This transient is so called partial permeation build-up or desorption transient. Results from partial build-up or desorption transient show that:

- In partial desorption transient followed after intermediate build-up, experimental curve did not overlap with the theoretical curve using solution of 2nd Fick`s law (Fourier or Laplace transformation) as shown in figure 35.

- In partial build-up transient without intermediates desorption; on the other hand gave a different picture in which the pre-charged membrane experimental permeation transient and the computer fitted theoretical transient overlapped each other.

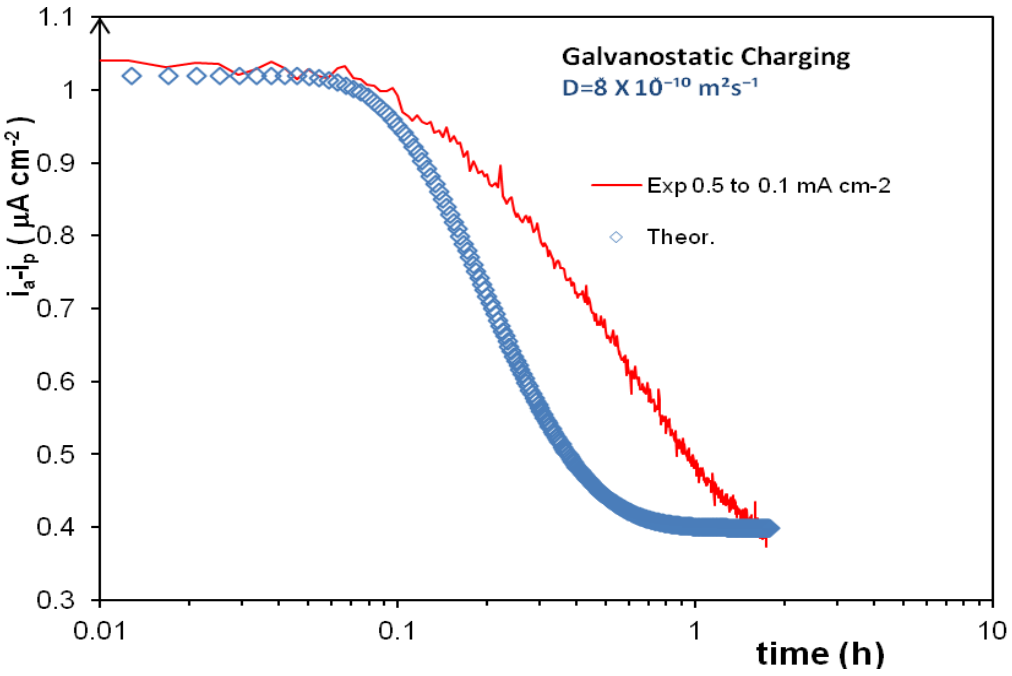

Figure 35: partial desorption transient with changing current of 0.5 to 0.1 mA cm^{-2}.

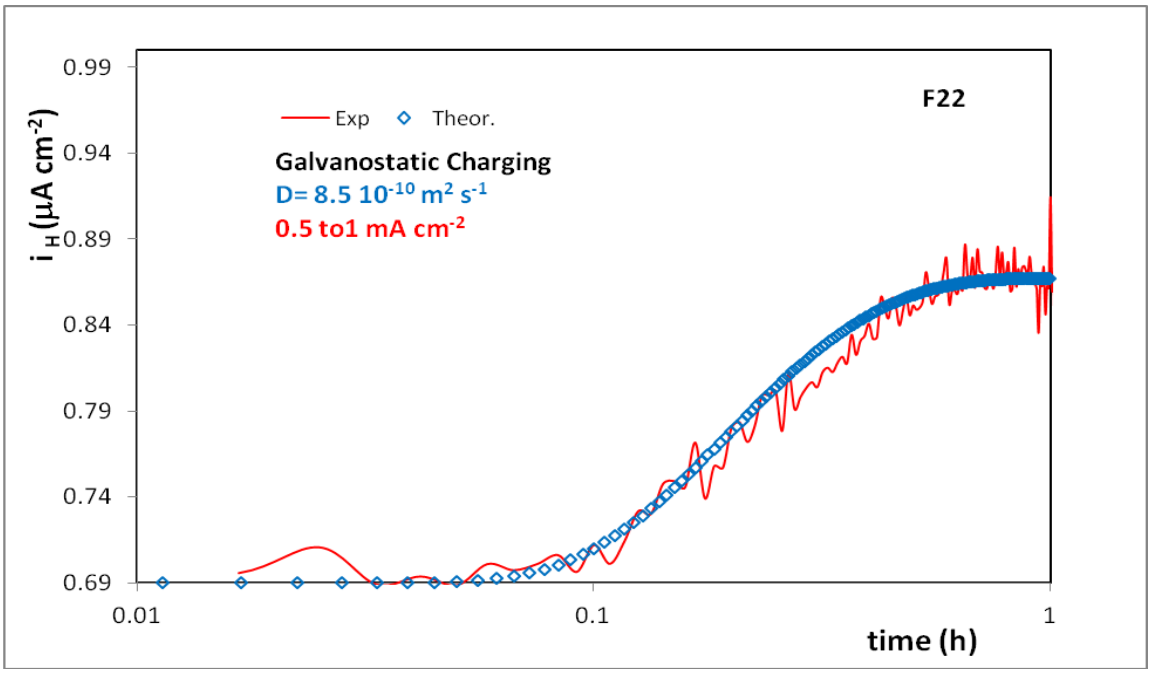

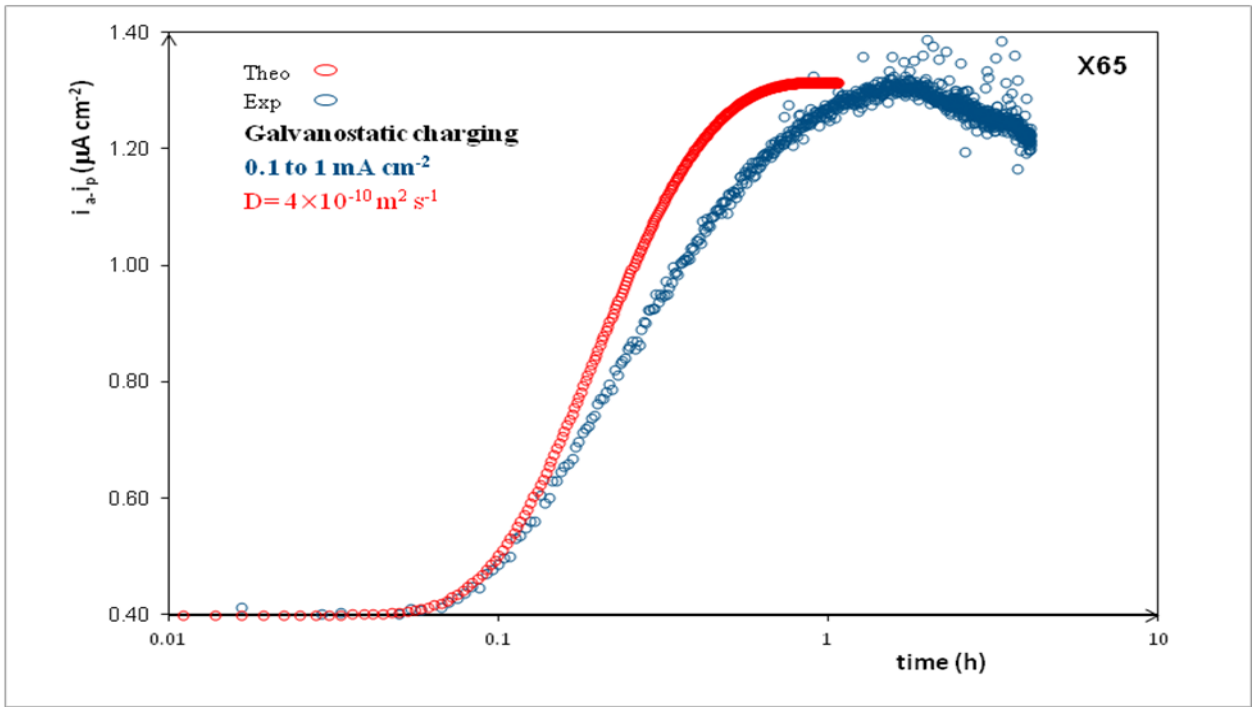

Figure 36: Figure: partial permeation build-up transient of pre-charged F22 and X65 specimen

This is a clear indication that with a change of the cathodic potential, the concentration C_o is changed immediately to a new constant value and the permeation of hydrogen is really controlled by its lattice diffusion through the membrane. The value of the lattice diffusion coefficient, D_L obtained by computer fitting procedure for F22 and X65 is in the range of 1 to 4 X 10^{-10} m^2s^{-1}, one order of magnitude higher than D_{app}.

D_L is used to plot the theoretical desorption curve. The anodic desorption rate, which was calculated using equation 84 and 85, was plotted alongside. A comparison of these curves is shown in figure 37. Since the total decay reflects the release of lattice hydrogen C_L and reversible trapped hydrogen C_{Tr}, their quantities can be calculated. The area A, between theoretical and experimental curve corresponds to the amount of C_{Tr}, while the area B, represent the amount of C_L. The hydrogen concentration C_H within these areas A or B, in $\mu A \frac{s}{cm^2}$, can be expressed in ppm Wt according to the equation.

$$C_H = A \frac{M_H}{FL\rho_{Fe}} \qquad (101)$$

Where F is the faraday constant (96,485 c/mol), M_H is the molar mass of hydrogen (1g/mol) and ρ_{Fe} is the density of iron.

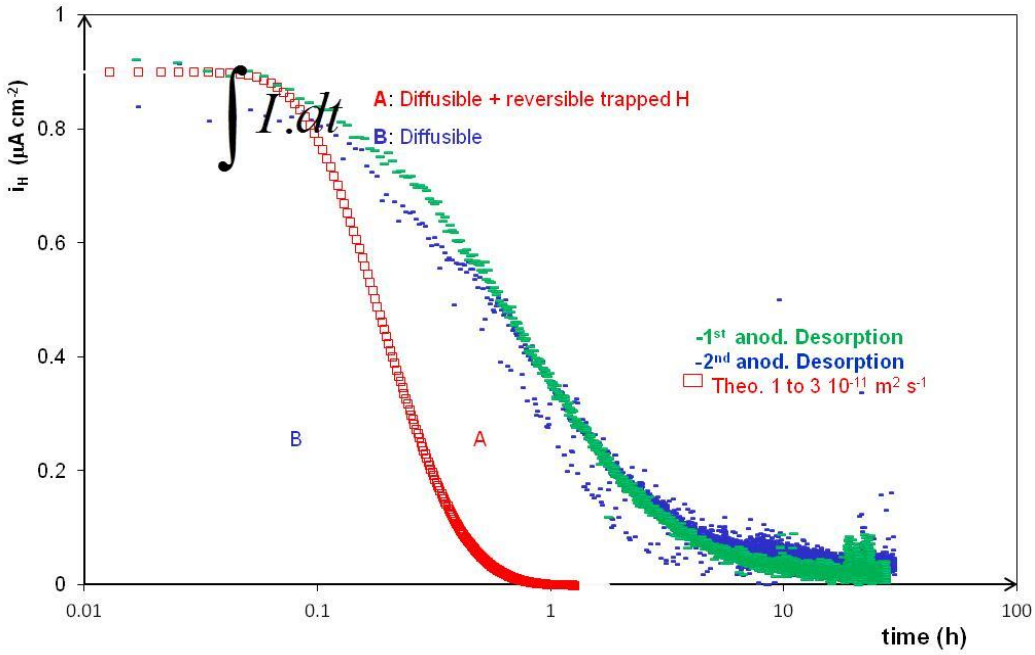

Figure 37: A complete desorption transient of the first and second desorption and the theoretical curve.

Table 8: hydrogen desorption analysis.

X65	$Q_{x=L}$ (C)	Q_{total} (C) from t_b (C_0*V/2)	$Q_{x=L}$ / Q_{tot}
1	0.04	0.17	0.24
2	0.03	0.14	0.21
3	0.02	0.08	0.25

F22	$Q_{x=L}$ (C)	Q_{total} (C) from t_b (C_0*V/2)	$Q_{x=L}$ / Q_{tot}
1	0.03	0.07	0.42
2	0.04	0.12	0.33
3	0.03	0.09	0.33

The amount ($Q_{H\ at\ X=L}$) of hydrogen extracted from the anodic side during hydrogen desorption can be estimated by measuring the area beneath the decay current-time curve. Comparing this value with $Q_{H\ Tot}$ (subsurface hydrogen concentration), to obtain the ratio $Q_{H\ at\ X=L} / Q_{H\ Tot}$, shown in table 8. The value of this ratio obtained varied slightly from the theoretical limit of 0.33 (corresponding to lattice diffusion) at a constant experimental condition. Thus, it can be concluded that the expected behavior, which was theoretically predicted for the exiting profile of hydrogen from the anodic and cathodic side are satisfied.

The hydrogen balance, according to figure 38, in a hydrogen charged membrane in terms of the total amount of the diffusible hydrogen and that of the trapped hydrogen showed that reversible trapped hydrogen for F22 is 90% and 72% for X65. These composed a majority in the total amount of absorbed hydrogen.

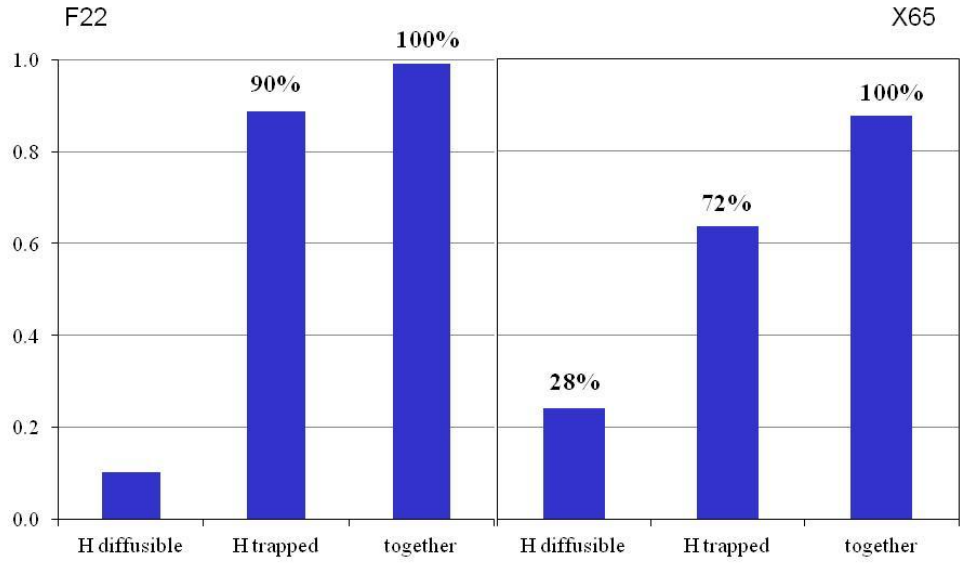

Figure 38: Hydrogen balance in F22 and X65 specimen.

Conclusion

The apparent diffusion coefficient evaluated at 40˚C by elaborating the permeation current density vs time curve with the different methods proposed in literature (time lag, time to breakthrough, rise time constant) is in the same range, 1 - 4×10^{-11} m^2 s^{-1}, of those one obtained at 20˚C. The expected ratio of the diffusion coefficient between 20 and 40°C on the basis of the activation energy is 1.5, same order of magnitude of the scattering of the results.

Lattice diffusion coefficient decreases with the time of the test. The fast and then slow trend that affect the diffusion of hydrogen might be correlated to the effect of trapping during the permeation.

Partial permeation transient, namely the partial build up obtained without intermediate discharge, can better estimate the lattice diffusion of hydrogen. Apparent hydrogen diffusion coefficient for both steels were one order of magnitude higher than the apparent diffusion coefficient.

The comparison betweeen the first and second permeation transient showed that sometimes at 40°C the second transient was faster than the first one, so it can be hypothesised an effect of irreversible traping; this effect was not recorded in the tests carried out at 20°C in previous phases of the research.

It has been confirmed also at 40°C that during the desorption on the anodic side the amount of hydrogen desorbed from this side is about 1/3 of the total, as in the previous experiments at 20°C.

The reversible trapping effect has been estimated by means of the desorption transient: the amount of hydrogen trapped in reversible sites (vs hydrogen contained in the lattice) was estimated in F22 up to 90% whereas this value was 77% for X65 steel sample.

Appendix

Figure x: Selected 1st and 2nd permeation transient obtained from different specimens as shown below, which covered the entire range of minimum and maximum permeation current obtained from experimental data (Fxxx = material F22; Xxxx = material X65).

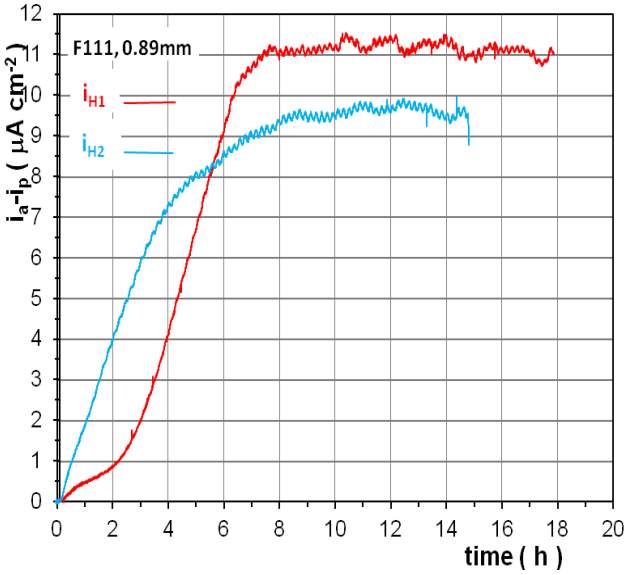

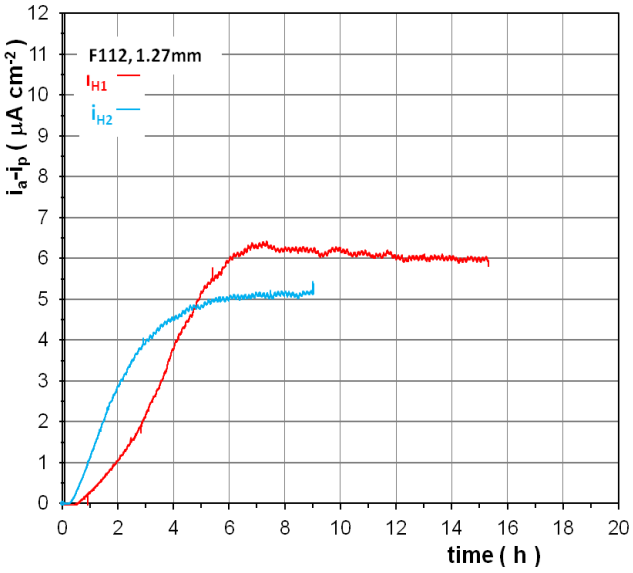

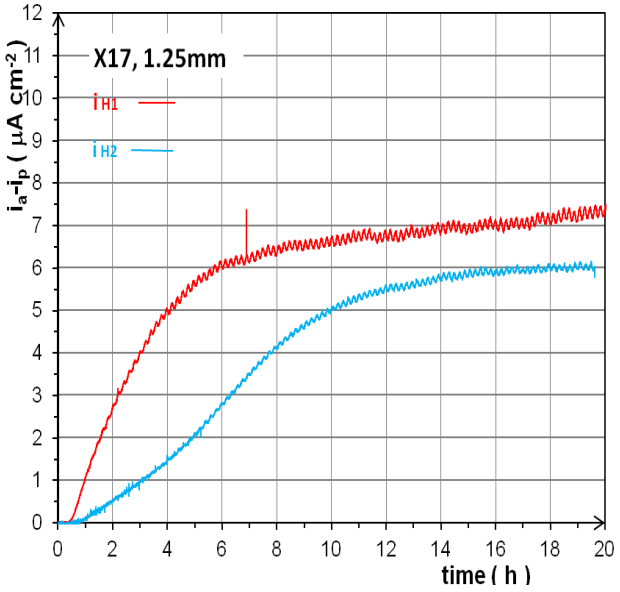

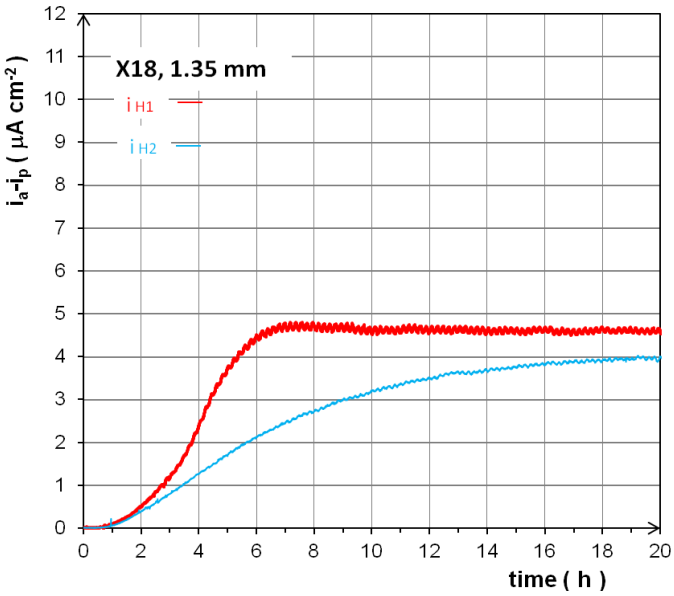

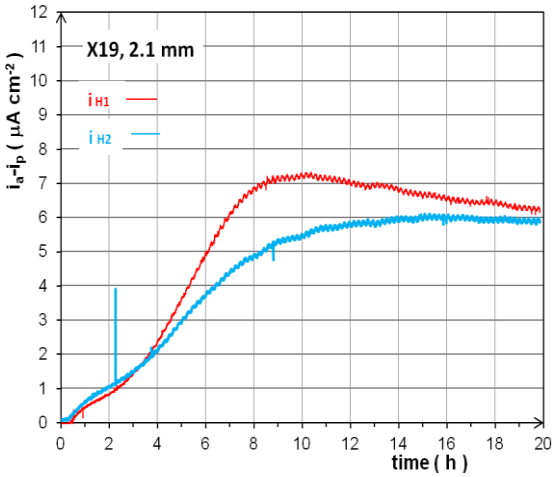
X19, 2.1 mm
i H1
i H2
i_a-i_p (µA cm-2)
time (h)

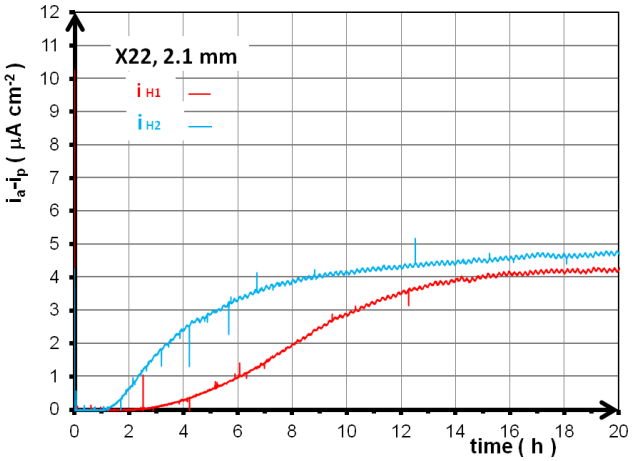
X22, 2.1 mm
i H1
i H2
i_a-i_p (µA cm-2)
time (h)

Table X: Selected results of D_{app} and C_o for F22 and X65 (1st and 2nd transient)

Specimens	**Tran**	$D_b(1\%)$ (m^2s^{-1})	$C_o(ppm)$	$D_b(10\%)$ (m^2s^{-1})	$C_o(ppm)$	$D_T(\tan gent)$ (m^2s^{-1})	$C_o(ppm)$
F22							
F111(0.89)	1st	2.90E-11	4.47	6.12E-12	21.45	-	-
	2nd	4.40E-11	2.55	2.88E-11	3.91	-	-
F19(1.2)	-	1.50E-11	6.91	1.19E-11	8.86	1.84E-11	5.73
F110(1.27)	1st	1.60E-11	12.43	1.05E-11	19.36	2.06E-11	9.84
	2nd	3.00E-11	9.65	1.95E-11	8.64	3.77E-11	4.47
F114(1.1)	-	1.40E-11	5.78	7.85E-11	10.43	2.07E-11	3.95
F115(1.3)	-	2.40E-11	4.94	2.45E-11	4.79	2.63E-11	4.46
F112(1.27)	1st	1.60E-11	12.43	1.05E-11	19.36	2.06E-11	9.84
	2nd	3.00E-11	5.65	1.95E-11	8.64	3.77E-11	4.47
X65							
X17(1.25)	1st	1.90E-11	5.21	1.26E-11	7.83	2.54E-11	3.90
	2nd	1.63E-11	6.68	1.27E-11	8.57	1.96E-11	5.55
X18(1.35)	1st	2.57E-11	3.31	1.77E-11	4.81	2.88E-11	2.95
	2nd	2.28E-11	5.22	1.64E-11	7.28	2.36E-11	5.06
X19(2.1)	1st	1.96E-11	6.12	1.78E-11	6.74	2.21E-11	5.43
	2nd	3.77E-11	3.70	4.45E-11	3.14	4.42E-11	3.16
X22(2.1)	1st	2.27E-11	4.29	1.01E-11	9.64	4.43E-11	2.20
	2nd	3.00E-11	2.63	1.62E-11	4.87	4.38E-11	1.80
X110(1.3)	-	4.69E-11	2.63	1.93E-11	6.39	7.41E-11	1.66
X111(0.86)	-	3.91E-11	1.30	2.44E-11	2.08	3.99E-11	1.27

List of figures

List of Tables

Bibliographic references

[1]: L. Nanis, T. K. G. Namboodhiri, Electrochemical Science and technology, Vol. 119, No. 6, Pp. 693-694, Giugno 1972.

[2]: NACE, Sulphide stress cracking metallic material for oil field equipment, NACE MR0175, 2003.

[3]: R. A. Oriani. ICCF4, The physical and metallurgical aspect of hydrogen in the metals. fourth International Conference on cold fusion,1993.

[4]: S. Duval, R. Antano-Lopez, C. Scomparin, M. Jerome, F. Ropital, Corrosion 2004, paper 04740.

[5]: ISO 17081:2004 (E), ISO, Switzerland, 2004

[6]: E. Fallahmohammadi, G. Fumagalli, G. Re, F. Bolzoni, L. Lazzari. Study on hydrogen diffusion in pipeline steels. Proceeding of Eurocorr, sweden (2011)

[7]: George Krauss, Sandre J. Midea, Heat treatment; steel heat treating including in the new millennium, 1999 [http://books.google.it/books?id=cYzNYwMtQHcC&pg=PA550&lpg=PA550&dq=causes+of+hydrogen+trappings+on+steel&source=bl&ots=6A-U9pXfs2&sig=5ymV6r3Y6B6kg2HtrVbJUOs9Q2U&hl=it&ei=1XelTuLZF4_dsga95dCYDA&sa=X&oi=book_result&ct=result&resnum=10&sqi=2&ved=0CIABEOgBMAk#v=onepage&q&f=false Pp. 540-570]

[8]: R. A. Oriani. ACTA metallurgica. Vol. 18. 1970,Pp 147-156

[9]: C. Zheng, Temperature effect on Hydrogen permeation of X56 steel, Materials Performance, April 2011.

[10]: Y. F. Cheng, Analysis of electrochemical hydrogen permeation through X-65 pipeline steel and its implications on pipeline stress corrosion cracking, 2006.

[11]: S. Frappart, X. Feaugas, J.Creus, F. Thebault, L.Delattre, H.Marchebois. Journal of physics and chemistry of solids 71 (2010) 1457-1479

[12]: [Joshua Lamb, Venugopal Arjunan. The Minerals, Metals and Materials society and ASM international. (2007)]

[13]: Nestor Perez. Electrochemistry and corrosion sci. Kluwer academic Publishers, 2004.

[14]: Guidelines on materials requirements for carbon and low alloys steels for H2S containing environments in oil and gas production. European Federation of corrosion publications.No.16.pp 15-27.2002

[15]: Luciano Lazzari, Encyclopedia of hydrocarbons, Chapt. 9.1, Pp 485-500.

[16]: DP Ghosh. Wet H_2S cracking problem in oil refinery processes- material selection and operation control issues. Tri-Science corrosion conference 2007

[17]: I.M. Robertson and H.K. Birmbaum. Acta mat. Vol. 47, No. 10, pp. 2991-2998, 1999.

[18]: H. Matsui, H.Kimura. Mat. Sci. and Eng. Vol. 40, Issue 2, 1979.pp 207-216

[19]: Janusz Flis. Corrosion of metals and hydrogen-related phenomena. Chapt. 7-10, Pp. 224-318, 1991.

[20]: M. Nagumo, H. uyama and M. yoshizawa. Accelerated failure in high strength steel by alternating hydrogen charging potential. Dept. of Mat. Sci. and Eng. Waseda Uni. Okubo, Tokyo. 2000.

[21]: J. O. M. Bockris, on hydrogen damage and the electrical properties of interfaces, pp. 286-304.

[22]: Valbona Hoxha, Enkela Nocka. Natura montenegrina, Podgorica, 10(2), Pp.149-155.

[23]: [Jai-Young Lee, U-in Chung. The effect of Phosphorus on the hydrogen trapping at grain boundaries in low carbon steel, Dept of mat. Sci. and eng, Korea Advanced Institute of sci. and tech. 2003.]

[24]: Fabio Bolzoni, Luciano Lazzari, H_2S and low temperature influence on toughness of carbon and low alloy steel, state of the art. Dept of chem. And Mat. Eng. Giulio Natta. 2008. Internal Report.

[25]: Fraser King. Hydrogen Effects on Carbon Steel Used Fuel Containers, Nuclear Waste management organization.Toronto. 2009-29

[26]:
[http://www.imoa.info/moly_uses/moly_grade_alloy_steels_irons/hydrogen_embrittlement.php]

[27]: C.M. Liao, J.L. Lee, Corrosion 50 (1994) 695.

[28]: Tadeusz Zakroczymski. Journal of Electroanalytical Chemistry 475 (1999), Pp. 82-88

[29]: W. Beck, diffusion and solubility of hydrogen as a function of composition in Fe-Ni alloy, Metallurgical Transcriptions, Vol. 2, 1971

[30]: M. A. V. Devanathan and Z. Stachurski. Proceedings of the royal society. 1962.

[31]: P. Fassina,F. Bolzoni,G. Fumagalli, L. Lazzari, L. Vergani, A. Sciuccati. Influence of Hydrogen and Low Temperature on Pipeline Steels Mechanical Behaviour. Procedia Engineering, (2011).

[32]: A. McNabb and P. K. Foster. Transactions of the metallurgical society of AIM. Vol 227. 1963

[33]: M. Lino. Acta. Metal. Vol 30. Pp. 367-375. 1982

[34]: J. B. Leblond and D. Dubois. Acta. Metall. Vol. 31. No 10. Pp. 1471-1478. 1983

[32]: Y. Sakamoto, T. Maintain, Effect of quenching and tempering on diffusion of hydrogen in carbon steel, 1976.

[33]: M. Cabrini, La metallurgia Italiana, 2008.

[34]: J. Kittel, New insights into hydrogen permeation steel; Measurement through thick membranes, Paper No. 8409.

[35]: H. J. Garbke, Adsorption and diffusion of hydrogen in steel, ISSN 1580-2949

[36]: A. Turnbull, Corrosion Science, Vol. 29, No. 1, Pp. 89-104, 1989

[37]: H. Addach, Study of Electrochemical permeation of hydrogen in iron, Corrosion Science, 51, 2009.

[38]: A. Turnbull, Acta Metallurgica, Vol. 37, No. 7, Pp. 2039-2046, 1989.

[39]: Andrea Monti, Tesi di Laurea Specialistica, Facolta di Ingegneria dei Processi Industriali, Dept. di Chi., Mat. e Ingegneria Chi., “Giulio Natta” 2011.

[40]: P. Fassina, F. Bolzoni, G. Fumagalli, L. Lazzari, L. vergani, A. Sciuccati, Engineering Fracture Mechanics, 81 (2012) 43-55.

[41]: Kane R. D, Cayard M. S, Roles of H2S in the behavior of engineering alloys; a revision of literature and experience-corrosion, 1998, Pp No 274

[42]: Gyu Tae park, Sung Ung Koh, Hwan Gyo Jung, Kyoo Young Kim, Corr. Sci. 50(2008), Pp. 1865-1871